Biomarker evidence for an MIS M2 glacial-pluvial in the Mojave Desert before warming and drying in the late Pliocene

Mark D. Peaple[1*], Tripti Bhattacharya[2], Jessica E. Tierney[3], Jeffrey R. Knott[4], Tim K. Lowenstein[5], Sarah J. Feakins[1]
[1]Department of Earth Sciences, University of Southern California, Los Angeles, CA 90089, USA.
[2]Department of Earth and Environmental Sciences, Syracuse University, Syracuse NY 13210, USA.
[3]Department of Geosciences, University of Arizona, Tucson, AZ 85721, USA.
[4]Department of Geological Sciences, California State University–Fullerton, Fullerton, California 92834, USA
[5]Department of Geological Sciences and Environmental Studies, State University of New York, Binghamton, New York 13902, USA
Correspondence to: M.D. Peaple, peaple@usc.edu

Key points

- Lacustrine sediments in Mojave Desert sediment core span 3.373–2.706 Ma.
- Microbial biomarkers record deep, fresh lake during cool period 3.373–3.268 Ma.
- Lake salinity increases after 3.268 Ma, associated with warming.

Abstract

Ancient lake deposits in the Mojave Desert indicate that the water cycle in this currently dry place was radically different under past climates. Here we revisit a 700 m core drilled 55 years ago from Searles Valley, California, that recovered evidence for a lacustrine phase during the late Pliocene. We update the paleomagnetic age model and extract new biomarker evidence for climatic conditions from lacustrine deposits (3.373–2.706 Ma). The MBT'_{5Me} temperature proxy detects present-day conditions (21 ± 3 ºC, n = 2) initially, followed by warmer-than-present conditions (25 ± 3 ºC, n = 17) starting at 3.268 and ending at 2.734 Ma. Bacterial and archaeal biomarkers reveal lake salinity increased after 3.268 Ma likely reflecting increased evaporation in response to higher temperatures. The $\delta^{13}C$ values of plant waxes (-30.7 ± 1.4‰, n = 28) are consistent with local C_3 taxa, likely expanded conifer woodlands during the pluvial with less C_4 than the Pleistocene.

δD values (-174 ± 5‰, n = 25) of plant waxes indicate precipitation δD values (-89 ± 5‰, n = 25) in the late Pliocene are within the same range as the late Pleistocene precipitation δD. Microbial biomarkers identify a deep, freshwater lake and a cooling that corresponds to the onset of major Northern Hemisphere glaciation at marine isotope stage MIS M2 (3.3 Ma). A more saline lake persisted for ~0.6 Ma across the subsequent warmth of the late Pliocene (3.268 to 2.734 Ma) before the lake desiccated at the Pleistocene intensification of Northern Hemisphere Glaciation.

Plain Language Summary

During a generally warm period three million years ago, there were large lakes in the Mojave Desert, California. We measured organic matter preserved in ancient lake mud below today's salt flat in Searles Valley to investigate the climate changes that sustained these three-million-year-old lakes. We compiled evidence for a freshwater lake, increased rainfall, and woody plants around the lake during a cooler interval, with similar-to-modern temperatures, that interrupted what was generally a warm period between five and three million years ago. Today the valley contains a saltpan, the evaporated remains of the former lake, surrounded by open desert shrubland. We compare the evidence from the lake with other climate reconstructions and find the wetter conditions coincided with cooling both locally and at higher latitudes.

1. Introduction

Multiple lines of evidence suggest that southwestern North America has become drier in recent decades and that this trend may be exacerbated by the further rise in CO_2 concentrations over 400 ppmv this century (Seager et al., 2007; Williams et al., 2020).

The Pliocene was the last time greenhouse gas concentrations were above 400 ppmv (Martínez-Botí et al., 2015) and the climate at that time may help contextualize current and future anthropogenic warming. The late Pliocene (Piacenzian) was the focus of PlioMIP Phase 1 (Haywood et al., 2013) and Phase 2 (Haywood et al., 2020) experiments that simulated climate during the mid-Piacenzian warm period (mPWP) between 3.264 and 3.025 Ma (De Schepper et al., 2013). Earth system models estimate global temperatures were 3.2 ºC warmer than preindustrial on average (range: 1.7–5.2 ºC), with on average 4.3 ºC warming over land and drying or modest wetting for southwestern North America (Haywood et al., 2013, 2020). The same climate models disagree about the sign of precipitation change associated with future warming in southwestern North America (Almazroui et al., 2021; Choi et al., 2016; Solomon et al., 2009).

Geological evidence for former lakes across the arid landscape of southwestern North America has long been of interest as they document wetter climate states (e.g., Russell, 1885). Lake shoreline features preserved on the landscape are typically those of the last highstand and recessional shorelines with only rare examples of multiple shorelines preserved (Jayko et al., 2008). In the Searles Valley basin, which includes both Searles and Indian Wells valleys, Pleistocene shorelines delineate the margins of a lake extending over 995 km^2 with a volume of 79.4 x 109 m^3 (Smith, 2009). Lake sediment cores from several valleys have revealed a continuous time series of fluctuations in sedimentary geochemistry, however all but one core retrieve sediments that are Pleistocene age (e.g., Smith, 1991).

Pliocene lake sediments crop out to a limited extent in several valleys east of the Sierra Nevada, California, including Death Valley (Knott et al., 2008), Searles Valley (Rittase et al., 2020), Fish Lake Valley (Reheis et al., 1993), and Eureka Valley (Knott et al., 2019) (**Figure 1**). From this same region, Pliocene sediment cores are only available from the KM-3 core of Searles Valley (Liddicoat et al., 1980; Smith et al., 1983). Interpretation of the core sediments indicate that Searles Valley experienced several lake highstands that overflowed the sill several times since the Pliocene (Jannik et al., 1991). Searles Valley contains a dry lake bed with evaporite deposits spanning the Holocene, atop deposits of lake muds deposited during Pleistocene pluvials and evaporites formed during drier periods (Knott et al., 2021; Olson et al., 2023; Olson & Lowenstein, 2021; Smith, 2009). The wettest times of the last 200 ka coincided with terminations T2 and T1 following the last two glacial maxima of marine isotope stages (MIS) 6 and 2 (Peaple et al., 2022; Stroup et al., 2023). Plant wax δD data (Peaple et al., 2022) corroborate independent evidence from cave carbonate $\delta^{18}O$ for precipitation isotopes (Lachniet et al., 2014; Moseley et al., 2016), lending confidence to these archives of past precipitation change. Archaeal and bacterial biomarkers captured late Pleistocene evidence for changing lake salinity in Searles Lake (Peaple et al., 2021, 2022) and nearby Lake Elsinore (Feakins et al., 2019). These salinity indicators have not yet been applied to Pliocene deposits, although they were first developed in Miocene deposits (Turich & Freeman, 2011). Temperature reconstructions using bacterial lipids are more commonly applied to lake sediments and have been successfully used in Pliocene reconstructions from Lake El'gygytgyn, northeastern Russia (Keisling et al., 2017), but not yet to any North American lacustrine deposits of Pliocene age.

In this study, we return to the late Pliocene sediments drilled from Searles Valley, previously studied for geochronology, mineralogy, and sedimentology (Liddicoat et al., 1980; Smith et al., 1983) long before these biomarker methods were established. Deep drilling (~1 km) within Searles Valley reached late Pliocene deposits and identified lacustrine conditions (Smith et al., 1983), making this one of the few continuous records on land in western North America capable of resolving temporal variability within the Pliocene (Thompson, 1991). Although the late Pliocene (Piancenzian) was globally warmer than today, a substantial cooling event was initially described from a benthic foraminifera oxygen isotope increase in deep sea sediments (Shackleton & Opdyke, 1977). This notable glacial event is named MIS M2 based on its timing in (and below) the Mammoth subchron (3.330–3.207 Ma; Ogg, 2020). The global benthic oxygen isotope increases, Icelandic margin marine evidence for ice-rafted debris, and glacial till in Canada, all appear in the lower Gauss subchron by 3.4 Ma (De Schepper et al., 2013), with cooling events MIS MG4 and MG2 preceding the deeper cooling of the M2 glaciation. Ice sheet modelling (Berends et al., 2019) and glacial deposits (Gao et al., 2012) indicate that a substantial ice sheet was present over the modern-day Hudson Bay and a smaller ice sheet was in place over the northern Cordillera but did not reach the Pacific coast (Sánchez-Montes et al., 2020). Although the glacial extent and degree of cooling has been debated, the M2 glaciation is now recognized to be a major glacial, redefined as the onset of Northern Hemisphere Glaciation before the later intensification at the Pleistocene boundary (McClymont et al., 2023). The extensive Laurentide ice sheet (LIS) during MIS M2 likely affected southwest North American climate, as ice cover has been shown to affect both winter and summer hydroclimate there (Oster et al., 2015; Lora et al., 2017; Bhattacharya et al., 2018). As originally noted by Liddicoat et al., (1980) the timing of the MIS M2 glaciation coincides with a perennial lake in Searles Valley, as well as lacustrine deposition in nearby Death Valley based on outcrop studies (Knott et al., 2018).

We sampled the continuous lacustrine sedimentary sequence from Searles Valley spanning the time corresponding to the MIS M2 glaciation and the extended warmth of the mPWP. We measured branched glycerol dialkyl glycerol tetraether (brGDGT) and isoprenoidal GDGT (isoGDGT) proxies to constrain changes in air temperature and lake salinity, and plant-derived biomarkers to reconstruct the δD of precipitation. We then compared the new data for the late Pliocene to prior reconstructions of the last two glacial and interglacial cycles (Peaple et al., 2022). With a few exceptions, we were able to measure the same suite of proxies, in sediments geologically over ten times older and collected 50 years before. This new record from Searles Lake constitutes a continuous terrestrial paleoclimate sequence of the late Pliocene, yielding evidence for temperature and hydroclimate in southwestern North America for comparison to regional and global climate change.

2. Study Location

2.1. Searles Valley tectonic context

Searles Valley episodically received inflow from the eastern flank of the Sierra Nevada via the Owens River during the late Pleistocene, and the same connectivity is thought to have persisted since the Pliocene (Blackwelder, 1933; Smith, 2009; Smith et al., 1983; **Figure S1**). Tectonics and topography are important both for orographic rainfall and drainage that form lakes. The Sierra Nevada may have uplifted at a fairly steady rate from the Oligocene to the Pliocene, with high rates of incision dated to before ~3 Ma by thermochronometry (Hammond et al., 2012; McPhillips & Brandon, 2010; Stock et al., 2004), perhaps explained by high runoff during a Pliocene pluvial. Cosmogenic nuclide dating, however, puts the incision later, primarily after 2.7 Ma (Stock et al., 2004), which could allow for incision primarily by glacial scouring in the Pleistocene. Uplift continued in the Pleistocene with the fastest rates in the northern Sierra Nevada (Hammond et al., 2012). The timing of uplift matters for the leeward sedimentary archives, such as Searles Lake, because later uplift scenarios could explain a drying trend unrelated to climate change in the Pliocene. A late uplift scenario could allow up to 50% more precipitation if the mountains were 1 km lower (Smith et al., 1983). However much global evidence for recent uplift (e.g., cooling, incision) may have been conflated with late Cenozoic climatic cooling (Molnar & England, 1990) and as such fluvial or glacial erosion may well explain Plio-Pleistocene Sierra Nevada incision. The consensus from precipitation isotopes in plant wax, carbonate, and tephra hydration is that an isotopic rainshadow (D-depletion) was in place by the middle Miocene (Hren et al., 2010; Mix et al., 2016, 2019; Mulch et al., 2008). Today, such D-depleted precipitation is associated with northerly moisture sources distilled by orographic processes crossing the northern and central Sierra Nevada (Friedman et al., 2002).

Tectonics within Searles Valley and adjacent basins may have also affected Pliocene basin connectivity. Lateral motion along the Marine Gate Fault (parallel to the now more active Garlock Fault, **Figure 1c**) resulted in several km of horizontal displacement between the deposition of the lacustrine facies and their present position (Rittase et al., 2020). During the Pliocene there is thought to have been some inflow from the south although the catchment may not have greatly expanded. At the eastern margin of Searles

Valley, radiometric evidence indicates rapid exhumation of the Slate Range from 6–4 Ma (Walker et al., 2014), with motion on the Searles Valley Fault (Rittase et al., 2020; **Figure 1c**). The deepening of the lake floor may have accompanied the uplift of the basin sides, although the resulting increased accommodation space would have been counteracted by the infilling of 300 m of lake sediment that accumulated between 3.4 to 2 Ma (**Figure 2**). If deepening and infilling were not smoothly aligned, this may have affected the lake storage capacity and potential for spillover into downstream basins. While the deep Pliocene Searles Lake sediments were interpreted as perennial lake deposits with persistent outflow (Smith et al., 1983), geomorphological evidence is inconclusive on whether outflow from Searles occurred in the Pliocene and what lake depth and volume could be contained within the evolving Pliocene basin (Knott et al., 2008). Although local tectonics may have had a transient influence on the potential volume of Pliocene Searles Lake, large contemporaneous lakes on the regional landscape robustly indicate a wet climate state (Knott et al., 2018; **Figure S1**).

2.2. Mojave Desert hydroclimate and vegetation

Today Searles Valley in the Mojave Desert has mean annual precipitation <100 mm/year, with sporadic rainfall dominantly occurring in the winter season (Western Regional Climate Center, 2022). High potential evaporation (~2,000 mm/year) in hot, dry and windy conditions means there is little to no surface water. Precipitation isotopes (δD_{precip}) reported from long-term sampling in Owens Valley (winter = -106‰, summer = -71‰), and modern groundwater in Owens Valley indicate dominantly winter recharge (Friedman et al., 1992, 2002), likely from spring melting of montane snowpack (Carrol et al., 2019). In southern Nevada, studies tracing the amount and isotopic composition of precipitation and groundwater indicate that in the lowlands too, winter precipitation contributes 90% of modern groundwater even though only 66% of precipitation occurs in winter (Winograd et al., 1998). As a result, most woody shrubs and trees across the region are deeply rooted to access consistent groundwater year-round rather than episodic rain. For example, *Juniperus osteosperma,* preferentially uses groundwater rather than summer rain (West et al., 2007). Combined ecohydrology and plant wax studies found that winter-recharge dominated groundwater is reflected in the δD of plant wax of most shrubs and trees across a coast-to-inland transect including the Mojave (Feakins and Sessions., 2010).

The vegetation of the lowlands is mostly desert shrubs with montane woodlands and forests on the Sierra Nevada. Packrat middens containing macrofossils allow for species level identification and show that *Juniperus osteosperma* woodlands expanded across the Mojave lowlands during Pleistocene pluvials (Holmgren et al., 2010; Koehler et al., 2005). Additionally, phreatophytic shrubs likely increased in Searles Valley during glacial periods (Peaple et al., 2022) possibly exploiting elevated groundwater levels. There are no published reports of Mojave paleovegetation for the Pliocene. At coastal marine core DSDP Site 467, 400 km to the west of Searles Valley, late Pliocene pollen record a similar-to-modern mixture of species including coastal oak-pine woodlands and chaparral vegetation (Ballog and Malloy, 1981; Heusser, 1981).

2.3. Sediment core and age model

We studied the Searles Lake sediment core KM-3 (USGS U234, well KM-3, 35.73371ºN, 117.32566ºW, 493 m asl) collected in 1968 by the Kerr-McGee Corporation and transferred to the US Geological Survey in 1976 (Liddicoat et al., 1980) and archived for

50 years in ambient, dry storage (USGS Core Research Center, Denver). We generated a Bayesian age model (Blaauw & Christen, 2011) for sediments from depths of 200–693 m (**Figure 2**) using previously identified paleomagnetic reversals (Liddicoat et al., 1980) and updated age estimates (Channell et al., 2020); dataset available at NOAA: Peaple et al., 2023) on the GPTS2020 timescale (Ogg, 2020).

The KM-3 core contains alluvial fill deposits above bedrock (Smith et al., 1983), suggesting that tectonics of the Slate range (Walker et al., 2014) allowed for basin development and fluvial deposition before the lacustrine phase. Using our updated age model, we studied Pliocene age sediments (3.373–2.706 Ma, 693–541 m depth, **Figure 2**) comprised of grey/brown thinly bedded mudstone (Hay et al., 1991; Smith et al., 1983) previously interpreted to be deep perennial lake facies (Unit I) (Smith et al., 1983). Here we investigate lacustrine changes using biomarker geochemistry evidence. From 3.373–2.706 Ma, the sediments had a relatively uniform sedimentation rate (0.22 m/ka), although the Mammoth and Kaena subchrons were characterised by higher sedimentation rates (0.26 and 0.32 m/ka, respectively). The onset of lacustrine conditions has coeval timing, within Pliocene dating uncertainties, in other basins of the Mojave Desert consistent with a wetter regional climate (Knott et al., 2018). Two regionally distributed tuffs (tuffs of Mesquite Flat and Zabriskie Wash) have been correlated with tuff deposits in the KM-3 core (681.5 m and 693.4 m respectively) (Knott et al., 2018), which provide a time-equivalent marker to link the lakes in Death Valley and Searles Valley and provide a secure basis for the timing of both lakes close to the Mammoth/lower Gauss boundary at 3.330 Ma.

Four paleomagnetic age boundaries between 3.330 and 3.032 Ma make this section well-dated (1 date/100 ka) compared to the rest of core KM-3, which aids comparison to proxy syntheses and model experiments for 3.264–3.025 Ma as part of PRISM (Pliocene Research Interpretation and Synoptic Mapping), PlioMIP (Pliocene Model Intercomparison Project) and PlioMIP2 (Haywood et al., 2016). In the Searles Lake paleomagnetic chronostratigraphy, there are three paleomagnetic tie points within the PRISM/PlioMIP window: Upper Kaena or C2An.1n(o) (616.2 m, 3.032 Ma GTS2020, 7.5 ka 1σ), Lower Kaena or C2An.1r9(o) (643.1 m, 3.116 Ma, 7.5 ka 1σ) and the Upper Mammoth or C2An.2r(y) (651.7 m, 3.207 Ma, 2 ka 1σ). In sediments younger than 2.9 Ma elevated lake salinity is implied by the diagenetic mineral anhydrite (which replaced the evaporite mineral gypsum). Beyond the extent of this study, soils sporadically formed in the basin 2.71–2.1 Ma (Smith et al., 1983). After 2.1 Ma fluctuating water availability led to interspersed deposition of evaporites and lacustrine muds (Smith et al., 1983).

3. Methods

3.1. Lipid extraction and separation

Lipids were extracted from 29 samples (~20 g) of freeze dried and homogenized sediments from core KM-3 by Accelerated Solvent Extraction (Dionex, ASE 350) using 9:1 dichloromethane (DCM):methanol (MeOH) at 100ºC and 1500 psi for 2 x 15 minute extraction cycles. Lipids were separated and purified following standard methods previously reported in detail for late Pleistocene sediments at Searles (Peaple et al., 2021). Briefly, the neutral and acid fractions were separated over aminopropyl sepra, the neutral fraction was separated into alkanes and GDGT fraction and further purified. The acid fraction was methylated overnight in methanol of known isotopic composition with

HCl to yield methyl esters and these were further separated by liquid-liquid extraction and purified by additional column chemistry prior to analysis.

3.2. Microbial biomarkers

The neutral polar fractions (containing GDGTs) were dissolved in hexane:isopropanol (99:1) and filtered through 0.45 μm polytetrafluoroethylene filters prior to analysis at the University of Arizona. GDGTs were separated using an Agilent 1260 High-Performance Liquid Chromatograph (HPLC) coupled to an Agilent 6120 mass spectrometer equipped with two Ethylene Bridged Hybrid (BEH) Hydrophilic Interaction (HILIC) silica columns (2.1 mm × 150 mm, 1.7 μm; Waters) following the method of Hopmans et al. (2016). Single Ion Monitoring (SIM) of the protonated molecules $(M + H)^+$ was used to detect and quantify GDGTs relative to a C_{46} internal standard (Huguet et al., 2006). Replicates were run to monitor reproducibility, to confirm that replicate precision is a trivial source of uncertainty. The largest uncertainty arises from the relative response factors between internal standard and analytes, which are unconstrained, thus concentrations should be considered semi-quantitative.

We quantified GDGTs, including the brGDGTs, derived from bacterial membrane lipids, and the isoGDGTs derived from archaea. Replicate analyses representing instrument precision indicate that uncertainty on quantification is less than 1%. In Pliocene sediments some peaks are below detection, and indices are not reported where the major components are not identifiable or the total peak area of the numerator or denominator falls below 3000. In addition to the concentration of individual compounds and summed totals (Σ) for each compound class, we calculate ratios that are informative about aspects of microbial production and limnological conditions. The relative abundance of individual compounds can be useful as indicators of microbial community and limnologic conditions. Crenarchaeol is produced uniquely by Thaumarchaeota (e.g., Sinninghe Damsté et al., 2002; Schouten et al., 2013) and is often abundant in oxic lakes (Baxter et al., 2021). While caldarchaeol (GDGT-0) is also produced by Thaumarcheota (e.g., Sinninghe Damsté et al., 2012b; Schouten et al., 2013), GDGT-0 without crenarchaeol implies water column anoxia and other producers including anaerobic methane-oxidizing archaea (Pancost et al., 2001; Schouten et al., 2001) and methanogenic Euryarchaeota (Schouten et al., 2013, and references therein). Although production of caldarchaeol in lake sediments has also been reported (Blaga et al., 2009), and as sediments are typically anoxic, anoxia cannot be confidently ascribed to the water column.

We calculate the archaeol caldarchaeol ecometric (ACE), a salinity index (Turich and Freeman, 2011), where:

$$\mathrm{ACE} = \frac{[archaeol]}{[archaeol]+[\mathrm{GDGT{-}0}]}\ x\ 100 \qquad (1)$$

As archaeol is dominantly produced by halophilic archaea, a higher ACE index is interpreted to represent more saline lake conditions (Turich and Freeman, 2011).

For the bacterial brGDGTs, the numbers I, II, and III refer to brGDGTs with four, five, and six methyl groups, and a, b, and c include zero, one, and two rings, respectively, the one two and three prime symbols (′) denote structural isomers with the methyl group at different positions. We calculate $\mathrm{IR}_{6+7\mathrm{Me}}$, an index sensitive to changes in lake salinity (H. Wang 2021)

$$IR_{6+7Me} = \left[\frac{IIa'+IIb'+IIc'+IIIa'+IIIb'+IIIc'}{IIa+IIb+IIc+IIIa+IIIb+IIIc+IIa'+IIb'+IIc'+IIIa'+IIIb'+IIIc'} + \frac{IIIa'''+IIa'''}{IIIa+IIIa'+IIIa'''+IIa+IIa'+IIa'''}\right] \times 0.5 \qquad (2)$$

The temperature-sensitive MBT′$_{5Me}$ index (De Jonge et al., 2014) is the relative methylation of the 5-methyl brGDGTs, where:

$$MBT'_{5Me} = \frac{[Ia+Ib+Ic]}{[Ia+ Ib+ Ic+IIa+IIb+IIc+IIIa]} \quad (3)$$

We use the Bayesian BayMBT$_0$ calibration of a global lake dataset (Martínez-Sosa et al., 2021) to convert MBT′$_{5Me}$ to the mean temperature of the months above freezing. We compare temperature and salinity reconstructions to examine the salinity-sensitivity of temperature reconstructions as high salinity in some lakes has been associated with a warm bias in the MBT′$_{5Me}$ proxy (Martínez-Sosa et al., 2021; Wang et al., 2021).

3.3. Plant wax biomarkers

The plant wax-derived *n*-alkanoic acids (analyzed as methyl esters from C_{16} to C_{32} carbon chain length), were quantified using an Agilent Gas Chromatograph Mass Spectrometer (GC-MS). We report concentrations for the individual *n*-alkanoic acids and compute the summed C_{22}-C_{32} *n*-alkanoic acid concentrations (Σalkanoic acid abundance) as well as carbon preference index (CPI) and the average chain length (ACL) calculated as:

$$\mathrm{CPI} = \frac{2[\mathrm{C_n}]}{[\mathrm{C_{n-1}}]+[\mathrm{C_{n+1}}]} \quad (4)$$

$$\mathrm{ACL} = \sum(\mathrm{n} \times [\mathrm{C_n}]) \sum[\mathrm{C_n}] \quad (5)$$

where the chain length (n) refers to the C_{22} to C_{32} *n*-alkanoic acids.

The *n*-alkanoic acid methyl esters were analyzed by Thermo GC equipped with a Triplus autosampler and a 30 m column (0.25 mm internal diameter, with a 0.25 μm type 5 coating) coupled via an Isolink (1000/1400ºC) for combustion or pyrolysis and Conflo IV to an isotope ratio mass spectrometer (GC-IRMS) and analyzed for C and H isotopic composition. Samples were injected with bracketing CO_2 and H_2 reference gases for comparison between sample and standard runs. Normalization of measured $\delta^{13}C$ and δD values to the international reference standards Vienna Pee Dee Belemnite and Vienna Standard Mean Ocean Water respectively was achieved with a multi-point organic reference standard containing C_{16}-C_{30} *n*-alkanes of known isotopic compositions (A6 mix supplied by A. Schimmelmann, University of Indiana; $\delta^{13}C$ values from −25.9 to −33.7‰ and δD values from −17 to −256‰). The RMS uncertainty for measured to known standard values for $\delta^{13}C$ and δD analyses was better than 0.1‰ and 5‰ respectively. Duplicate sample analyses have on average 0.03‰ and 2‰ instrument precision. Linearity was assessed daily across 1–8 V, for $\delta^{13}C$ (σ = 0.07‰), and for δD the linearity is applied as a correction (H_3^+ factor averaged 9.89 ppm/mV) the latter applied as a correction within Isodat. Reported $\delta^{13}C$ and δD values for *n*-alkanoic acids were corrected to account for the contribution of the methyl group (Lee et al., 2017).

Plant wax $\delta^{13}C$ and δD values were used to reconstruct vegetation and precipitation isotopic composition similar to previous applications to the late Pleistocene Searles Lake core studying both the *n*-alkanoic acids and *n*-alkanes (Peaple et al., 2022), as well as regional applications to Pleistocene (Bhattacharya et al., 2018; Feakins et al., 2019) and Pliocene sediments (Bhattacharya et al., 2022) all performed on *n*-alkanoic acids. Peaple et al., (2022) tested three different approaches to constrain possible vegetation effects on changing the appropriate fractionation ($\varepsilon_{wax/precip}$) in late Pleistocene Searles Lake including using pollen assemblages, machine learning on plant wax abundance distributions and the $\delta^{13}C$ of plant wax. The three methods of determining a varying $\varepsilon_{wax/precip}$ produced similar $\delta D_{precipitation}$ compared to the use of a constant $\varepsilon_{wax/precip}$ (Peaple et al., 2022), and therefore vegetation effects were not found to be a significant uncertainty in the late Pleistocene. In the Pliocene we have no constraints on vegetation change other than carbon isotopes. Large changes in the proportion of C_3 and C_4 grasses (and thus $\varepsilon_{wax/precip}$) are not supported by regional pollen studies (Ballog and Malloy, 1981; Heusser, 1981) and did not occur during Pleistocene glacial or interglacial periods (Peaple et al., 2022). C_4 and woody C_3 vegetation also have similar $\varepsilon_{wax/precip}$ (Sachse et al.,2012) and thus changes in the landscape proportion of these two plant groups is unlikely to significantly affect our δD precipitation reconstruction. Thus we applied the constant $\varepsilon_{wax/precip}$ of -93‰ (Feakins et al., 2014, 2019; Feakins & Sessions, 2010), where:

$$\delta D_{precip} = \frac{\delta D_{wax} + 1}{\varepsilon_{wax/precip} + 1} - 1 \quad (6)$$

This constant $\varepsilon_{wax/precip}$ is robust across different plant communities and aridity levels in modern environments in the region (Feakins and Sessions, 2010). While wetter climate states of the past may have resulted in larger $\varepsilon_{wax/precip}$ the transition point for any such changes are unconstrained, and this remains an uncertainty on δD_{precip} reconstructions.

The *n*-alkane fraction contains an uncharacterized complex mixture indicating a mature hydrocarbon contribution from degradation in situ, sedimentary migration of petrogenic hydrocarbons or contamination during drilling. The dominance of mature hydrocarbons in Pliocene sediments from KM-3 precludes consideration of plant wax *n*-alkanes, which has been the preferred plant wax precipitation isotope indicator in the late Pleistocene sediments (Peaple et al., 2022).

3.4. Pollen

Following standard pollen methodology as in a study of the late Pleistocene in this basin, we screened 1 cc of sediment from two initial samples selected at random from the 29 samples studied for biomarkers. While pollen was well-preserved in late Pleistocene sediments drilled in 2017 (Peaple et al., 2022), Pliocene-age samples from core KM-3 were barren of pollen. We have since learned that pollen was not found in initial surveys of the KM-3 core in 1976 as well during a second attempt in the late 1990s. We thus conclude core storage is not the issue, but rather degradation in situ in the last 3 Ma. We report the null result to save additional fruitless effort at palynology in core KM-3.

3.5. Statistics

3.5.1. Breakpoint analysis

We used the offline Power of the Pruned Exact Linear Time (PELT) (Wambui et al., 2015) method implemented in the Ruptures Python library (Truong et al., 2020). PELT is an exact search algorithm that uses a least squares deviation cost function to detect mean changes (changepoints) in our time series.

3.5.2. Intergroup differences

In order to determine if there are statistically significant differences between groups of samples, we used a two-sided non-parametric Kolmogorov-Smirnov test. Taking into account age uncertainty, we calculated the p value for the Kolmogorov-Smirnov for each Bacon age ensemble member to generate a distribution of p values. We then calculated the median p value of this distribution to establish whether groups are statistically different ($p < 0.05$).

4. Results

We present the biomarker results for the late Pliocene lacustrine deposits from the KM-3 core at Searles Lake (**Figure 3**) in the context of the limnological interpretation of Smith et al., (1983) (**Figure 3a**).

4.1. GDGTs

4.2. Concentrations

ΣisoGDGTs (2.01 ± 3.86 ng/g, n = 29) far exceed the concentrations of ΣbrGDGTs (0.07 ± 0.13 ng/g, n = 29) (**Figure 3c**), showing dominance of archaeal rather than bacterial production. Downcore spikes in abundance in both compound classes could be due to production, preservation or most likely reduced sedimentary dilution. While GDGTs were measured on all 29 samples, some compounds, especially some of the brGDGTs and crenarchaeol, were absent in some samples, limiting the availability of some of the derived indices.

4.3. Salinity indicators

Both salinity indicators are low from 3.373–3.268 Ma (**Figure 3d**) with ACE (40.6 ± 17.6%, n = 6) and IR_{6+7Me} (0.33 ± 0.04, n = 2) denoting lower salinities and fresh to brackish conditions. Higher ACE (57.3 ± 6.5%, n = 23) and IR_{6+7Me} (0.52 ± 0.02, n = 17) indicate saline conditions, including hypersalinity, from 3.268 to 2.706 Ma. In order to statistically evaluate if there are salinity differences between these two periods across both proxies, we calculated a two-sided Kolmogorov-Smirnov test for each age ensemble member generated from Bacon and then calculated the median p value from this ensemble. The median p values from the resultant p value ensembles for ACE and

IR_{6+7Me} (0.033 and 0.012) indicate that the salinity differences for these two intervals are statistically significant for both indicators, one bacterial, one archaeal, providing robust evidence for the salinity change.

4.4. Temperature proxies

MBT'_{5Me} indicates temperatures of 20 to 30 °C from 3.319 to 2.706 Ma using the $BayMBT_0$ lakes calibration (MAF, months above freezing) (Martínez-Sosa et al., 2021) (**Figure 3e**). Absence of brGDGTs IIa, Iib, Iic and IIIa in some samples precludes calculation of the bacterial temperature index MBT'_{5Me} especially in the early part of the record where brGDGTs concentrations are lowest. This may be because of low bacterial production or subsequent degradation. Although the data are sparse, the first two temperature estimates, dated to 3.319 and 3.268 Ma, yielded a mean temperature of 21 ± 3°C (compound 1σ uncertainty, n = 2), followed by a warming of 4 °C after 3.268 Ma to a mean temperature of 25 ± 3 °C (n =17) across 3.246–2.734 Ma. The temperatures from these periods are significantly different following our age uncertain Kolmogorov-Smirnov approach (Section 3.4.3).

4.5. Plant wax

4.6. Concentrations

Summed *n*-alkanoic acid (C_{22}-C_{32}) concentrations (Σalkanoic acid) averaged 11.0 ± 9.2 ng/g (n = 28). Σalkanoic acid concentrations are low (0.9 ± 0.5 ng/g, n = 6) before 3.221 Ma, thereafter, increasing to higher concentrations (13.8 ± 8.4 ng/g, n = 22) (**Figure 3f**). Visual inspection of smear slides showed a shift from coarser grains (sand) to finer grained (silt/clay) lithology at 3.221 Ma. Although not a quantitative comparison, coarse grained materials result in volumetric dilution of biomarkers, whereas finer grains provide more surface area for the preservation of organic matter. The carbon preference index (CPI) was consistently low (3.3 ± 0.3, n = 28). The average chain length (ACL) of the C_{22}-C_{32} alkanoic acids was slightly longer (27.4 ± 0.3, n = 4) before 3.268 Ma compared to after 3.268 Ma (26.1 ± 0.4, n = 24). Reduced ACL after 3.268 Ma may reflect a shift in aquatic macrophyte production or the terrestrial plant community (Peaple et al., 2021) and/or may suggest more microbial degradation in soils (Brittingham et al., 2017; M. S. Wu et al., 2019) during the warmer and drier climate.

4.7. Carbon isotopic composition

$\delta^{13}C$ values for the C_{28} *n*-alkanoic acids range from -31.6 to -27.0‰ (-29.2 ± 1.2‰, n = 28) and for the C_{30} *n*-alkanoic acids -34.0 to -28.4‰ (-30.7 ± 1.4‰, n = 28) (**Figure 3g**). The $\delta^{13}C$ values of the C_{30} *n*-alkanoic acids range from a high of -29.6‰ at 3.478 Ma, to a low of -34.0‰ at 3.200 Ma and then return to generally high values from 3.0-2.7 Ma with a high of -28.4‰ at 2.891 Ma.

4.8. Hydrogen isotopic composition

The δD values of the C_{28} *n*-alkanoic acids (-174 ± 6‰, n = 26) and the C_{30} *n*-alkanoic acids (-174 ± 5‰, n = 25), are the same within uncertainty, however the individual samples show variable offsets for the C_{28}-C_{30} (+10 to -17‰), perhaps source differences, or analytical noise. Applying the $\varepsilon_{wax/precip}$ regionally defined fractionation for plant wax *n*-alkanoic acids (Feakins et al., 2014, 2019), the measured δD values for C_{28} yield precipitation isotopic composition (δD_{precip}) estimates for the Pliocene interval (-89 ± 6‰, n = 26) and values calculated from C_{30} are equivalent (-89 ± 5‰, n = 25). Downcore variations of 22‰ (**Figure 3h**) do not covary with plant wax $\delta^{13}C$ or abundance distributions so appear robust to plant type and preservation. The δD values may thus carry signals of hydroclimate or heterogeneous catchment erosional inputs.

5. Discussion

5.1. Lake depth reconstruction

Lake depth in terminal lakes is inversely related to water salinity, as evaporation leaves behind the salts delivered by river inflow. Smith et al. (1983) originally depicted lacustrine sedimentation as evidence for a consistently deep lake from 3.4 to 2.6 Ma (dates updated to the current timescale; **Figure 3a**). However, this was apparently a simplification as they also described the diagenetic mineral anhydrite (which replaced gypsum) at depths of 681.8 to 546.2 m, indicating the precipitation of evaporite minerals in sediments younger than 2.9 Ma (**Figure 3a**), which implies saline lake conditions. Anhydrite-rich sandstones, indicating saline waters, were also reported by Hay & Guldman (1987) at depths of 656.6 to 640.2 m. We report new biomarker evidence for saline lake waters (**Figure 3d**) that lead to a revised interpretation (**Figure 3a**) consistent with adjacent lake basins. These biomarker-based salinity reconstructions are derived from different microbial lineages: the ACE and the IR_{6+7Me} salinity proxies and are calculated from the lipids of archaea and bacteria respectively, known for detection of hypersaline and brackish water lakes respectively (Turich and Freeman, 2011; H. Wang et al., 2021) and applied to Pleistocene salinity variations in this lake basin (Peaple et al., 2022). While the bacterial and archaeal communities are unknown for the (former) Searles Lake, each has its own salinity tolerance ranges and environmental sensitivities, based on paleoenvironmental comparisons in the Pleistocene sediments in the SLAPP-SRLS17 core (Peaple et al., 2022) and the sampling of modern conditions in Asian lakes (H. Wang et al., 2021). Here, during the cool-temperature phase (**Figures 4e**) both ACE and IR_{6+7Me} proxies (**Figures 4f-g**) are low consistent with lower salinity and brackish, perennial lake conditions. We detect increases in the IR_{6+7Me} at 3.268 Ma and this coincides with local warming detected by $BayMBT_0$ (**Figure 4e**) and global warming into the late Pliocene warm period (**Figure 4a and b**). The ACE salinity index has a step change increase after 3.14 Ma (**Figure 4f**), which lags the change observed in the IR_{6+7Me} record (**Figure 4g**) possibly due to the low sensitivity of ACE at low salinities (Peaple et al., 2022; H. Wang et al., 2021) or some temperature sensitivity in the IR_{6+7Me}. The dual archaeal and bacterial biomarker evidence for increasing salinity reported here, together with the anhydrite noted by Smith et al., (1983), each provide independent confirmation for a saline lake during the mPWP.

In this late Pliocene reconstruction we found crenarchaeol to be at vanishingly low abundance, being undetectable in many samples, with just 3 samples having crenarchaeol as more than 1% of the ΣisoGDGTs (0.5 ± 1.1%, n = 29; **Figure S2**). However, GDGT-0 was high, thus Searles Lake was likely mostly anoxic and stratified, similar to the majority of the last 200-ka reconstruction (Peaple et al., 2022). In contrast, during Termination 2 at the end of MIS 6, crenarchaeol relative abundance peaked at 16% of ΣisoGDGTs and GDGT-0 was low, which was interpreted as a vigorously overturning deep lake phase (Peaple et al., 2022). That interpretation is supported by geomorphic evidence for spillover into downstream Panamint Valley (Jayko et al., 2008). This suggests that the Termination 2 pluvial was wetter than the MIS M2 pluvial. One caveat about the late Pliocene and late Pleistocene comparison is that microbial communities may have changed over the intervening 3 Ma and there is some evidence for this. Alkalinity increased in the basin following hydrothermal activity in the vicinity of the

Long Valley volcanic center (Lowenstein et al., 2016) and this was associated with a change in the microbial community at Searles Lake as evidenced by carotenoids before and after 1.4 Ma (Winters et al., 2013).

5.2. Mojave pluvial associated with MIS M2 glaciation

The evidence for a deep lake in Searles Valley associated with the MIS M2 glacial was first described and dated by Liddicoat et al. (1980). Here we updated the timing of the paleomagnetic datums (**Figure 2**) and sampled the lacustrine phase to refine interpretations with new biomarker evidence. We find that older sediments (3.373–3.268 Ma) associated with the MIS M2 glacial (3.312–3.264 Ma) capture relatively cool conditions (**Figure 4e**), and relatively fresh lake waters as detected by semi-quantitative, independent bacterial and archaeal indicators (**Figure 4f, g**), compared to the relative warmth (mean 25 ºC) and salinity rise of the subsequent mPWP (**Table 1**). There are significant differences ($p<0.05$) for temperature and salinity between periods 3.370–3.264 Ma and 3.264–2.950 Ma which broadly align with the high latitude MIS M2 cooling (cooling includes the precursor cooling of MG 4 and 2, **Figure 4b**, as identified by changepoint analysis here) and extended mPWP warm periods respectively.

Corroboration of pluvial conditions associated with the extended MIS M2 glacial cooling comes from regional comparison. The onset of lacustrine deposition at 3.4 Ma at Searles Lake, corresponds to a perennial lake in nearby Death Valley (**Figure 4a**), together indicating a considerable P-E increase (Knott et al., 2018). Searles Lake records a climate (MAF mean = 20.7 ºC ± 0.3 ºC, n = 2; **Figure 5**) similar to or slightly warmer than the modern (MAF = 20 ºC; **Figure 5**), and much warmer than Pleistocene glacial maximum periods (MAF = 17.4 ± 1.8, n = 11; Peaple et al., 2022; **Figure 5**). Compared to the past two glacial maxima, the higher potential evaporation during M2 implies much more precipitation was a necessary condition for the lake to fill. The fresh, deep lake is robust evidence for cooler and wetter conditions in southwestern North America associated with the extended cooling including the late Pliocene MIS M2 glaciation, that we refer to as the “M2 pluvial”, compared to drier conditions during the mid-Pliocene warmth.

We note that changes in salinity have the potential to impact MBT'_{5Me} based temperature reconstructions (Martinez-Sosa et al., 2021; Wang et al., 2021). Modern observational studies of the nearby Mono Lake have found that the core top MBT'_{5Me} based temperature reconstructions are too warm when compared to modern temperatures (25.5 ºC versus 10.6 ºC respectively), possibly due to low production of lake derived brGDGTs (Martinez-Sosa et al., 2021) or differing ecological communities relative to the calibration. However, MBT'_{5Me} was found to be relatively insensitive to changes in salinity in Searles Lake over the past 200 ka (Peaple et al., 2022). $BayMBT_0$ temperature interpretations were corroborated by independent evidence from the Brillouin approach applied to evaporite minerals across the last 40 ka (Olson et al., 2023). We also note that $BayMBT_0$ temperatures discern reasonable glacial and interglacial temperature offsets as well as Pliocene M2 glacial and mPWP offsets (**Figure 5**) compared to the modern months above freezing mean temperature. These observations and plausible temperature reconstructions support the assumption that MBT'_{5Me} is dominated by changes in temperature in the Pliocene and Pleistocene. We cannot rule out that changes in salinity have had a secondary effect on temperature reconstruction, or that changes in salinity influenced IR_{6+7Me}, as there is some similarity between the structure of the IR_{6+7Me} salinity and the $BayMBT_0$ temperature reconstructions for the Pliocene, both derived from bacterial brGDGTs (**Figure 3c and d**). In particular, the inferred warming into the mPWP coincides with an inferred salinity increase such that warm-bias in saltier conditions is a concern, although these two phenomena should be related as warming likely led to increased evaporation and salinity.

5.3. Understanding climate and drivers of the M2 pluvial

A limitation with understanding the climate response to the MIS M2 glacial is the sparse terrestrial evidence available to date. Additional terrestrial reconstruction efforts would ideally add evidence in future, however Pliocene lacustrine sedimentary accumulations persist only in rare basins on land. Arguably, the best terrestrial archive of this time is Lake El'gygytgyn (northeastern Russia). There, a 10 ºC cooling from peak mid-Pliocene warmth to near-Holocene temperatures from 3.39 to 2.64 Ma (**Figure 4c**) was inferred from pollen evidence for a shift from boreal forest to tundra (Brigham-Grette et al., 2013). That cooling in northeastern Russia is detected by change-point analysis here (**Figure 4b**) coincident with a cooling detected in marine benthic $\delta^{18}O$ into MIS MG4 about 0.1 Ma prior to the MIS M2 glaciation (Westerhold et al., 2020).

Marine sedimentary records spanning the Pliocene are more readily available, and nearby to the Lake El'gygytgyn record, alkenones capture a 6 ºC cooling of SSTs from the Gulf of Alaska (**Figure 4d**) with the cooling also beginning at 3.4 Ma and reaching a minimum during MIS M2. The absence of ice-rafted debris, however, indicates that the Cordilleran ice sheet did not reach all the way to the coast (Sánchez-Montes et al., 2020). The cooling is most pronounced in high latitudes, closer to the locus of terrestrial glaciation, but the California Current propagates the signal southward to Site 1012 (32.2ºN, offshore the US-Mexico border) with a 4 ºC cooling recorded by alkenones

(Brierley et al., 2009). The magnitude of cooling along the coastal ocean is consistent with terrestrial cooling of 4 ºC at Searles Lake (35.7ºN) – the cooling here is relative to the later mPWP, as our record begins in the cool interval.

Globally, the MIS M2 glacial from 3.312–3.264 Ma was accompanied by a $\delta^{18}O$ increase of 1.1‰ according to the latest estimates (Westerhold et al., 2020; **Figure 4b**) revised upwards from the initial evidence of 0.4‰ (Shackleton & Opdyke, 1977) and 0.5‰ (Lisiecki & Raymo, 2005). Estimates of a 20–60 m sea level drop relative to today were associated with the smaller $\delta^{18}O$ shifts, whereas lower sea levels are likely associated with the 1.1‰ increase. However, Mg/Ca and clumped isotope temperature reconstructions of the Atlantic and Pacific indicate that a large 4°C drop in bottom water temperature occurred during the M2 glacial (Braaten et al., 2023), which indicates that ice volume increases were reduced compared to Pleistocene glacial maximums. The main uncertainties on these foraminiferal estimates of glacial magnitude arise from diagenesis concerns (Raymo et al., 2018), although foraminiferal preservation improved in samples from MIS M2 (De La Vega et al., 2020).

The MIS M2 glacial cooling was accompanied by a 100 ppmv decrease in atmospheric carbon dioxide similar to that of late Pleistocene glacials, with evidence from $\delta^{11}B$ of foraminifera indicating a drop from 400 ppmv to 300 ppmv (De La Vega et al., 2020). The high-resolution record finds that the drop in pCO_2 lagged the orbital and $\delta^{18}O$ oscillation, thus another mechanism for the initiation of the glacial event is required. That trigger may have been the re-opening of the shallow Central American Seaway altering circulation between the Pacific and Atlantic and thus the heat flux to the high latitude Atlantic Ocean (De Schepper et al., 2014; Tan et al., 2017).

Model experiments to test sensitivity during the MIS M2 glaciation find only the large ice sheet scenario produces a measurable change in precipitation and drying in southwestern North America (Dolan et al., 2015). The modelled drying is at odds with the evidence for a pluvial presented here. Given that late Pleistocene glacial conditions are associated with pluvials in the southwest, we posit that similar mechanisms could have operated in the Pliocene (Fu, 2023; Lofverstrom, 2020; McGee et al., 2018a). Further elucidation of the climate dynamics will have to await additional MIS M2 simulations that succeed in representing the glacial-pluvial conditions.

5.4. Drying and warming into the mPWP

After the MIS M2 glacial, we find evidence for warming and drying at the start of an extended warm phase, the mPWP (**Figure 4d**). The warm period spanning 3.264–3.025 Ma (MIS M1 through MIS G21) is the focus of PRISM and a series of PlioMIP model and proxy intercomparisons. We report new terrestrial brGDGT-based paleothermometry evidence that Searles Valley was 4 ºC warmer during the mPWP than during the M2 event. Mean Searles Valley temperatures were slightly warmer during the mPWP compared to the last interglacial (MAF = 24.3 ºC vs 22.4 ºC respectively; **Figure 5**), indicating that Searles must have been receiving much more precipitation than modern, given the presence of a perennial lake.

Globally, annual mean temperatures were around 3.5 ºC higher in the mPWP warm period than today (Burke et al., 2018; Dowsett & Caballero Gill, 2010; Haywood et al., 2020; Ravelo et al., 2004). Consistent with global warmth during the mPWP, we find mean reconstructed mPWP MAF temperatures at Searles Lake (24 ± 3 ºC, n = 5). Although terrestrial quantitative temperature estimates remain rare, supporting evidence for warming comes from diatom assemblage studies from Tule Lake, northern California (**Figure 1**), that found *Aulacoseira solida* abundances increased coincident with the mPWP before an increase in *Fragilaria* spp. denoting cooling likely associated with the intensification of Pleistocene Northern Hemisphere glaciation (Thompson, 1991). A local warming of 4 ºC from M2 into the mPWP would imply a higher evaporation rate than currently exists in Searles Valley. Today Searles Valley lowland receives 100 mm/year precipitation, with ~2000 mm/year potential evaporation. During pluvials with inflowing Owens River, the catchment included the eastern Sierra Nevada which has modern precipitation of around 400 mm/year (Lake Sabrina, Western Regional Climate Center., 2022). Menemenlis et al. (2022) performed calculations for the southern Great Basin region; in their wettest scenario they estimate that sustaining a 18.6% lake coverage would require 1.0 mm/day (2.5x) more rainfall across the broad region, given a similar-to-modern temperature regime. As the spatial heterogeneity of a mountain catchment is not well represented by such a calculation, and as the large regional areas of lakes in the northern reaches of their study area are beyond the scope of this study, we cannot directly relate their calculations to Searles Lake. We do not attempt lake water balance calculations for Searles Lake as the volume of the Pliocene basin is unclear, but a doubling of modern precipitation to fill a deep lake seems plausible.

Referring again to the southern Great Basin calculations for the dry and intermediate scenario of Menemenlis et al. (2022), with 1.6 and 3.6% lake coverage, then a saline lake could imply up to 0.4 mm/day (1.2x) more precipitation over the broad region compared to today. Downscaling quantitative reconstructions of basin water balance and climate for Searles Lake must await refinement of the basin size as well as a realistic treatment of precipitation change across the topography of the catchment in climate models. However, the Searles Lake proxy data are consistent with wetter-than-modern conditions during the mPWP to produce the intermittent/saline lake, under elevated temperatures, however conditions were drier than in the M2 pluvial.

5.5. Carbon isotopic reconstructions

$\delta^{13}C$ values for the *n*-alkanoic acids indicate a trend of ^{13}C-depletion across chain lengths from C_{24} to C_{30}. The isotopic spread likely relates to shifting proportions of various producers of long-chain *n*-alkanoic acids, with measured variations among terrestrial plants in the region, as well as possible macrophyte inputs (Peaple et al., 2021). We show the C_{28} *n*-alkanoic acids (-31.6 to -27.0‰) and C_{30} *n*-alkanoic acids -34.0 to -28.4‰ (-30.7 ± 1.4‰, n = 28; **Figure 3g**), with C_{30} being most ^{13}C-depleted and most likely indicative of terrestrial plants.

These carbon isotopic values are consistent with the trees and shrubs sampled in the modern catchment, with *n*-alkanoic acid production likely dominated by the coniferous taxa, with $\delta^{13}C$ values of -29.7‰ for *Juniperus occidentalis*, -24.7‰ for *Abies concolor,* and -25‰ for *Pinus jeffreyi* (Peaple et al., 2022). Coniferous taxa tend to produce plant wax with a high proportion of *n*-alkanoic acid to *n*-alkanes (Diefendorf et al., 2011), as also measured in local trees (Peaple et al., 2021) and fluvial runoff (Feakins et al., 2019). Conifers expanded their lowland range in cooler, wetter times of the Pleistocene based on macro- and microfossils (Wolfenden, 2003; Holmgren et al., 2010; Koehler et al., 2005; Peaple et al., 2022). However, the $\delta^{13}C$ values of the *n*-alkanoic acids were not significantly different between the last glacial maximum and interglacial of the late Pleistocene. While conifers may have also expanded into the lowlands during the M2 pluvial, the $\delta^{13}C$ values of the *n*-alkanoic acids are not significantly different from that of the mPWP, with both high and low values in each interval. Overall, the $\delta^{13}C$ values of the *n*-alkanoic acids are lower in this late Pliocene record than the late Pleistocene (Peaple et al., 2022).

The *n*-alkanes and pollen together provided evidence for varying proportions of C_4 phreatophytic shrubs (including Atriplex) during the Pleistocene (Peaple et al., 2022). However *n*-alkanes and pollen are not preserved in these Pliocene sediments rendering vegetation largely unknown for the Pliocene in this basin. We note the M2 glacial drop in pCO_2 was from 400 to 300 ppmv (De La Vega et al., 2020). Thus atmospheric conditions would have been less favorable for C_4 than during the late Pleistocene glacials, which were another 100 ppmv lower at 180 ppmv (Petit et al., 1999).

Coeval with warming and drying into the mPWP, we find an increase in *n*-alkanoic acid $\delta^{13}C$ (from -34 to -28‰) across 3.4–2.9 Ma. We note a positive correlation between lake salinity, as measured by ACE and $\delta^{13}C_{wax}$ (C_{30} $r = 0.51$, $p = 0.05$ and C_{28} $r = 0.45$, $p = 0.15$) accounting for serial correlation (Ebisuzaki, 1997). The range of values is consistent with open C_3 vegetation in the region today (Peaple et al., 2022), and so the shift may indicate range changes among those species: perhaps Pinus expansion into higher elevations after the M2 glacial, and a reduction in Juniper in the lowlands due to drying. In addition, the $\delta^{13}C$ increase may indicate an increase in moisture stress among C_3 plants (Diefendorf et al., 2010). Alternatively, the trend could indicate C_4 plant contributions. Similar carbon isotope enrichment trends in the late Pliocene have been reported from soil carbonates, from Camp Rice, New Mexico (Mack et al., 1994), and from St. David, Arizona, where the trend represents C_4 grassland expansion reflecting warming and summer (North American Monsoon; NAM) rainfall (Y. Wang et al., 1993). Recent proxy and modeling work suggest that the NAM may have expanded into southern California during the mPWP (Fu et al., 2022; Bhattacharya et al., 2022), which could lead to C_4 expansion. However, the vegetation of the Mojave lowlands and Sierra Nevada watershed remains an open question until in situ Pliocene paleobotanical macro or microfossil clues are found.

5.6. Precipitation isotope reconstructions

The δD_{precip} reconstruction for Searles Lake in the late Pliocene does not show any change between the M2 glacial pluvial and the mPWP, nor from the Pleistocene (**Figure 3h**). δD_{precip} reconstructions based on *n*-alkanoic acids for 3.373 to 2.706 Ma from KM-3 (-89 ± 5‰, n = 25, this study) are 10‰ more D-depleted than reconstructions from SLAPP-SRLS17 spanning 200 to 4 ka (-77 ± 18‰, n = 112; Peaple et al., 2022). These reconstructions are the same within uncertainties given the different sample size, temporal variability and sampling resolution. Each of these Searles Lake *n*-alkanoic acid δD_{precip} reconstructions fall within the seasonal means of the modern climatology. In the late Pleistocene δD reconstruction, the *n*-alkanes were the preferred compound class, reflecting the expected pattern of glacial D-depletion and interglacial D-enrichment seen in the *n*-alkanes and in other regional reconstructions (Peaple et al., 2022). Whereas the *n*-alkanoic acid evidence was deemed less useful through comparisons in the Pleistocene (Peaple et al., 2022), with downcore variability perhaps confounded by changes in conifer elevation and macrophyte inputs (Peaple et al., 2021), the Pliocene plant wax reconstructions therefore must remain tentative.

Independent evidence for δD_{precip} values during the MIS M2 glaciation, has previously been reported from the Owens River watershed (Mulch et al., 2008), part of the Searles Valley catchment. Using the waters of hydration extracted from the Nomlaki Tuff (ca. 3.30 Ma; Knott et al., 2018) sampled in Fish Lake Valley, Mulch et al. (2008) estimated δD_{precip} was -144‰ when the Nomlaki Tuff was deposited. Mulch et al. (2008) hypothesize that the hydration rinds of the volcanic glass shards formed within 10^3 -10^4 years after eruption and deposition, and thus the δD values integrate MIS M2 glacial precipitation. The δD_{precip} from hydration of tephra indicates winter-precipitation dominated the MIS M2 glacial adjacent to the Searles Valley catchment. The -144‰ value of the hydrated glass shards is more D-depleted than modern mean annual precipitation, but is similar to values recorded during high precipitation winter storms in the Southern Great Basin (Friedman et al., 1992, 2002).

Today the Searles Lake catchment receives dominantly winter orographic precipitation passing over or leaking to the south of the Sierra Nevada with rare summer rain much of which is lost to evaporation (Friedman et al., 2002). In the Pliocene evidence indicates precipitation was also dominated by winter storms distilled over the Sierra Nevada (Mulch et al., 2008) and tentatively corroborated by our plant wax *n*-alkanoic acid evidence. Although regional summer monsoonal rains increased in intensity (Bhattacharya et al., 2022), they likely reflected a minor contribution to the Searles Lake catchment. The isotopic evidence east of the Sierra Nevada (tephra, plant wax) requires only an increase in the number rather than seasonality or trajectory of storm tracks delivering the P-E excess filling large lakes during the MIS M2 glacial pluvial. The M2 pluvial was followed by relatively drier conditions during the mPWP although still requiring more rain than today to sustain a perennial lake. In the modern climate of

California, inter-annual variability is linked to a few extra extreme storms, with the wettest 5% of days explaining 1/3 of the annual precipitation but 2/3 of the variance with most of this falling on the Sierra Nevada (Dettinger, 2016). Similarly, the receipt of a few more extreme storms each year, could explain a pluvial phase that filled Searles Lake, lasting 150 ka around the MIS M2 glacial cooling.

Further south, in what is now the Anza Borrego Desert (31.4°N), 400 km south of Searles and 100 km inland from the Gulf of California and Pacific Ocean, a petrified laurel-willow-walnut forest of late Pliocene age required increased precipitation and incursions of coastal fog (Remeika et al., 1988). However, ODP Site 1012 (**Figure 1**) marine core isotopic evidence suggests summer rather than the originally proposed winter-season precipitation increase (Bhattacharya et al., 2022). In that study, plant wax reconstructions from marine core sites ODP Site 1012 and DSDP Site 475 (**Figure 1**) found δD_{precip} values were 20‰ heavier than modern across 3.5–3 Ma, consistent with a strengthened North American Monsoon (NAM) (Bhattacharya et al., 2022). They linked strengthened NAM to reduced subtropical to equatorial eastern Pacific SSTs in the warmer background state of the late Pliocene (that study did not have the temporally resolution to detect any perturbation associated with the MIS M2 glacial cooling). A strengthened NAM would likely have increased summer precipitation over Searles Lake at the northwestern edge of the modern NAM region (Western Regional Climate Center., 2023). Currently, the Searles Catchment receives only 10% of its mean annual precipitation during the NAM months of July, June, and August (Western Regional Climate Center., 2023) and much of this is lost to evaporation, not reaching groundwater or plants (Carroll et al., 2020). However, modeling of the NAM expansion (Fu et al., 2022; Bhattacharya et al., 2022) suggests a substantial incursion of summer rainfall is possible for the mPWP, suggesting that summer rain could have contributed to the higher Searles lake levels. In addition, if summer humidity increased substantially, summer evaporative losses would decrease and the water may have become more available to plants and groundwater recharge.

5.7. Climate dynamics during the MIS M2 glacial pluvial

Although ice sheet extent is not well constrained for the Pliocene MIS M2 glaciation globally, or for the Cordilleran Ice Sheet (Sánchez-Montes et al., 2020), the LIS extended over the modern-day Hudson Bay (Gao et al., 2012; Berends et al., 2019). The sizable LIS during the MIS M2 glaciation, would have depressed the winter storm track southward leading to an increased moisture flux to the mid-latitudes. We hypothesize that the Pliocene MIS M2 glaciation may have yielded more inland penetrating atmospheric rivers with similar dynamics to those of the modern climate (Rutz et al., 2015) due to similar topography, but with greater frequency or amount of moisture transported to explain the filled lake basins. Although we invoke similar mechanisms to the late Pleistocene glacial pluvials, the 30x longer duration of the extended M2 pluvial merits further investigation.

Prior efforts to understand the climate of late Pliocene warmth have integrated time-slabs and this may have resulted in an under-appreciation of the orbital-scale variability within the late Pliocene (Prescott et al., 2014). This has been hypothesized to be behind some of the proxy-model disagreement (Haywood, et al., 2013). The biomarker reconstruction from Searles Lake core KM-3, provides clarification that the pluvial conditions were associated with MIS M2 glaciation (and cooling associated with the MG4 and MG2 precursors) followed by drier conditions within the mPWP (**Table 1**), although still wetter than modern conditions. We hope the new biomarker evidence can refresh interest in modelling the MIS M2 glacial (Dolan et al., 2015), to elucidate the climate dynamics that explain the pluvial conditions, reconstructed here.

6. Conclusions

Applying biomarker proxies to sediments from the KM-3 core of Searles Valley, California, we have demonstrated variable lacustrine conditions during the late Pliocene, a period previously interpreted as a continuously deep lake (Smith et al., 1983). Continuous sedimentation and a lacustrine record through the Mammoth reversal subchron make Searles Lake a valuable subtropical (35.7ºN) terrestrial archive of conditions during the MIS M2 glacial. We find that the MIS M2 glacial was locally a cool pluvial, with a deep lake from 3.4 to 3.2 Ma consistent with other interpretations (Knott et al., 2018; Liddicoat et al., 1980). Warming into the mPWP led to a saline lake that persisted for ~0.6 Ma before desiccation. The biomarker salinity evidence is corroborated by a positive shift in carbon isotopes of plant waxes as well as prior observations of evaporites in the lake sediments (Smith et al., 1983).

Intense pluvial conditions of the late Pliocene co-occurred with a cooling around the MIS M2 glaciation that interrupted warmth, much like the pluvial states of the late Pleistocene. As we reconstruct similar to modern temperatures during MIS M2 at Searles Lake, evaporation would also have been similar to modern, and thus the P-E surplus necessary to fill a deep lake must have be dominated by increased rainfall (Ibarra et al., 2018). During the subsequent warmth of the mPWP, the persistence of a perennial lake implies more rainfall than present to yield a P-E surplus, although less rainfall than during the M2 pluvial. Additional studies are needed to add spatial and temporal resolution to the nature of the climate transitions across the MIS M2 glacial and mPWP.

Acknowledgments

The biomarker study and GRA (Peaple) were supported by U.S. National Science Foundation Grant NSF-EAR-1903665 to S.F., GDGT analyses were supported by the Packard Fellowship for Science and Engineering to J.T. and NSF-OCE-1903171 to J.T. T.B. was supported by NSF-OCE-1903148. JRK was supported by the National Science Foundation Integrated Earth Sciences grant EAR-1516593. Sample material used in this project was provided by the USGS Core Research Center. We thank Patrick Murphy for his assistance in preparing and measuring GDGTs. We thank colleagues for helpful discussions at Pliocene workshops including Peter Molnar, Erin McClymont, Bette Otto Bleisner and Alan Haywood. We thank Dan Ibarra, Ran Feng and Joe Liddicoat for reading earlier versions of the manuscript. This manuscript was improved with reviews from Associate editor Yige Zhang, two anonymous reviewers and Julie Brigham-Grette.

Open Research

Data files are publicly available and archived at the NOAA paleoclimatology database (Peaple et al., 2023).

References

Almazroui, M., Islam, M. N., Saeed, F., Saeed, S., Ismail, M., Ehsan, M. A., et al. (2021). Projected Changes in Temperature and Precipitation Over the United States, Central America, and the Caribbean in CMIP6 GCMs. *Earth Systems and Environment 2021 5:1*, *5*(1), 1–24. https://doi.org/10.1007/S41748-021-00199-5

Bacon, S. N., Jayko, A. S., Owen, L. A., Lindvall, S. C., Rhodes, E. J., Schumer, R. A., & Decker, D. L. (2020). A 50,000-year record of lake-level variations and overflow from Owens Lake, eastern California, USA. *Quaternary Science Reviews*, *238*, 106312. https://doi.org/10.1016/j.quascirev.2020.106312

Baxter, A. J., van Bree, L. G. J., Peterse, F., Hopmans, E. C., Villanueva, L., Verschuren, D., & Sinninghe Damsté, J. S. (2021). Seasonal and multi-annual variation in the abundance of isoprenoid GDGT membrane lipids and their producers in the water column of a meromictic equatorial crater lake (Lake Chala, East Africa). *Quaternary Science Reviews*, *273*, 107263. https://doi.org/10.1016/J.QUASCIREV.2021.107263

Berends, C. J., de Boer, B., Dolan, A. M., Hill, D. J., and van de Wal, R. S. W.: Modelling ice sheet evolution and atmospheric CO_2 during the Late Pliocene, Clim. Past, 15, 1603–1619, https://doi.org/10.5194/cp-15-1603-2019, 2019.

Besseling, M. A., Hopmans, E. C., Boschman, R. C., Sinninghe Damsté, J. S., & Villanueva, L. (2018). Benthic archaea as potential sources of tetraether membrane lipids in sediments across an oxygen minimum zone. *Biogeosciences*, *15*(13), 4047–4064.

Bhattacharya, T., Tierney, J. E., Addison, J. A., & Murray, J. W. (2018). Ice-sheet modulation of deglacial North American monsoon intensification. *Nature Geoscience*, 1. https://doi.org/10.1038/s41561-018-0220-7

Bhattacharya, T., Feng, R., Tierney, J. E., Rubbelke, C., Burls, N., Knapp, S., & Fu, M. (2022). Expansion and Intensification of the North American Monsoon During the Pliocene. *AGU Advances*, *3*(6). https://doi.org/10.1029/2022av000757

Braaten, A. H., Jakob, K. A., Ho, S. L., Friedrich, O., Galaasen, E. V., De Schepper, S., Wilson, P. A., and Meckler, A. N.: Limited exchange between the deep Pacific and Atlantic oceans during the warm mid-Pliocene and MIS M2 "glaciation", Climate of the Past. [preprint], https://doi.org/10.5194/cp-2023-13, in review, 2023.

Blaauw, M., & Christeny, J. A. (2011). Flexible paleoclimate age-depth models using an autoregressive gamma process. *Bayesian Analysis*, *6*(3), 457–474. https://doi.org/10.1214/11-BA618

Blackwelder, E. (1933). Lake Manly: An Extinct Lake of Death Valley. *Geographical Review*, *23*(3), 464. https://doi.org/10.2307/209632

Blaga, C. I., Reichart, G.-J., Heiri, O., & Sinninghe Damsté, J. S. (2009). Tetraether membrane lipid distributions in water-column particulate matter and sediments: a study of 47 European lakes along a north–south transect. *Journal of Paleolimnology*, *41*(3), 523–540.

Brigham-Grette, J., Melles, M., Minyuk, P., Andreev, A., Tarasov, P., DeConto, R., et al. (2013). Pliocene warmth, polar amplification, and stepped Pleistocene cooling recorded in NE Arctic Russia. *Science*, *340*(6139), 1421–1427.

Brittingham, A., Hren, M. T., & Hartman, G. (2017). Microbial alteration of the hydrogen and carbon isotopic composition of n-alkanes in sediments. *Organic Geochemistry*, *107*, 1–8. https://doi.org/10.1016/j.orggeochem.2017.01.010

Burke, K. D., Williams, J. W., Chandler, M. A., Haywood, A. M., Lunt, D. J., & Otto-Bliesner, B. L. (2018). Pliocene and Eocene provide best analogs for near-future climates. *Proceedings of the National Academy of Sciences*, *115*(52), 13288–13293.

Carroll, R. W., Deems, J. S., Niswonger, R., Schumer, R., & Williams, K. H. (2019). The importance of interflow to groundwater recharge in a snowmelt-dominated headwater basin. *Geophysical Research Letters*, *46*(11), 5899-5908.

Carroll, R. W., Gochis, D., & Williams, K. H. (2020). Efficiency of the summer monsoon in generating streamflow within a snow-dominated headwater basin of the Colorado River. *Geophysical Research Letters*, *47*(23), e2020GL090856.

Channell, J. E. T., Singer, B. S., & Jicha, B. R. (2020). Timing of Quaternary geomagnetic reversals and excursions in volcanic and sedimentary archives. *Quaternary Science Reviews*, *228*, 106114. https://doi.org/10.1016/J.QUASCIREV.2019.106114

Chiang, J. C. H., Lee, S. Y., Putnam, A. E., & Wang, X. (2014). South Pacific Split Jet, ITCZ shifts, and atmospheric North–South linkages during abrupt climate changes of the last glacial period. *Earth and Planetary Science Letters*, *406*, 233–246. https://doi.org/10.1016/J.EPSL.2014.09.012

Choi, J., Lu, J., Son, S. W., Frierson, D. M. W., & Yoon, J. H. (2016). Uncertainty in future projections of the North Pacific subtropical high and its implication for California winter precipitation change. *Journal of Geophysical Research: Atmospheres*, *121*(2), 795–806. https://doi.org/10.1002/2015JD023858

Curry, R. R. (1966). Glaciation about 3,000,000 years ago in the Sierra Nevada. *Science*, *154*(3750), 770–771.

Damsté, J. S. S., Weber, Y., Zopfi, J., Lehmann, M. F., & Niemann, H. (2022). Distributions and sources of isoprenoidal GDGTs in Lake Lugano and other central European (peri-) alpine lakes: Lessons for their use as paleotemperature proxies. *Quaternary Science Reviews*, *277*, 107352.

De Schepper, S., Groeneveld, J., Naafs, B. D. A., Van Renterghem, C., Hennissen, J., Head, M. J., et al. (2013). Northern hemisphere glaciation during the globally warm early late Pliocene. *PloS One*, *8*(12), e81508.

De Jonge, Cindy, Hopmans, E. C., Zell, C. I., Kim, J. H., Schouten, S., & Sinninghe Damsté, J. S. (2014). Occurrence and abundance of 6-methyl branched glycerol dialkyl glycerol tetraethers in soils: Implications for palaeoclimate reconstruction. *Geochimica et Cosmochimica Acta*, *141*, 97–112. https://doi.org/10.1016/j.gca.2014.06.013

Diefendorf, A. F., Freeman, K. H., Wing, S. L., & Graham, H. V. (2011). Production of n-alkyl lipids in living plants and implications for the geologic past. *Geochimica et Cosmochimica Acta*, *75*(23), 7472–7485.

Dolan, A. M., Haywood, A. M., Hunter, S. J., Tindall, J. C., Dowsett, H. J., Hill, D. J., & Pickering, S. J. (2015). Modelling the enigmatic Late Pliocene Glacial Event — Marine Isotope Stage M2. *Global and Planetary Change*, *128*, 47–60. https://doi.org/10.1016/J.GLOPLACHA.2015.02.001

Dowsett, H. J., & Caballero Gill, R. P. (2010). Pliocene climate. *Stratigraphy*, *7*(2–3), 106–110.

European Space Agency, Sinergise (2021). Copernicus Global Digital Elevation Model. Distributed by OpenTopography. https://doi.org/10.5069/G9028PQB. Accessed: 2023-05-02

Farquhar, G., & Richards, R. (1984). Isotopic composition of plant carbon correlates with water-use efficiency of wheat genotypes. *Australian Journal of Plant Physiology*, *11*(6), 539. https://doi.org/10.1071/PP9840539

Feakins, S. J., & Sessions, A. L. (2010). Controls on the D/H ratios of plant leaf waxes in an arid ecosystem. *Geochimica et Cosmochimica Acta*, *74*(7), 2128–2141. https://doi.org/10.1016/J.GCA.2010.01.016

Feakins, S. J., Kirby, M. E., Cheetham, M. I., Ibarra, Y., & Zimmerman, S. R. H. (2014). Fluctuation in leaf wax D/H ratio from a southern California lake records significant variability in isotopes in precipitation during the late Holocene. *Organic Geochemistry*, *66*, 48–59. https://doi.org/10.1016/J.ORGGEOCHEM.2013.10.015

Feakins, S. J., Wu, M. S., Ponton, C., & Tierney, J. E. (2019). Biomarkers reveal abrupt switches in hydroclimate during the last glacial in southern California. *Earth and Planetary Science Letters*, *515*, 164–172. https://doi.org/10.1016/j.epsl.2019.03.024

Friedman, I., Smith, G. I., Gleason, J. D., Warden, A., & Harris, J. M. (1992). Stable isotope composition of waters in southeastern California 1. Modern precipitation. *Journal of Geophysical Research*, *97*(D5), 5795. https://doi.org/10.1029/92JD00184

Friedman, I., Harris, J. M., Smith, G. I., & Johnson, C. A. (2002). Stable isotope composition of waters in the Great Basin, United States 1. Air-mass trajectories. *Journal of Geophysical Research: Atmospheres*, *107*(D19), ACL 14-1. https://doi.org/10.1029/2001JD000565

Fu, M., Cane, M. A., Molnar, P., & Tziperman, E. (2022). Warmer Pliocene upwelling site SST leads to wetter subtropical coastal areas: A positive feedback on SST. *Paleoceanography and Paleoclimatology*, *37*(2), e2021PA004357

Gagnon, C., Butler, K., Gaviria, E., Terrazas, A., Gao, A., Bhattacharya, T., et al. (2022). *Paleoclimate controls on lithium enrichment in Great Basin Pliocene-Pleistocene lacustrine clays*. https://doi.org/10.31223/X54D15

Gao, C., McAndrews, J. H., Wang, X., Menzies, J., Turton, C. L., Wood, B. D., et al. (2012). Glaciation of North America in the James Bay Lowland, Canada, 3.5 Ma. *Geology*, *40*(11), 975–978. https://doi.org/10.1130/G33092.1

Hammond, W. C., Blewitt, G., Li, Z., Plag, H. P., & Kreemer, C. (2012). Contemporary uplift of the Sierra Nevada, western United States, from GPS and inSAR measurements. *Geology*, *40*(7), 667–670. https://doi.org/10.1130/G32968.1

Hay, R. L., & Guldman, S. G. (1987). Diagenetic alteration of silicic ash in Searles Lake, California. *Clays and Clay Minerals*, *35*, 449–457.

Hay, R. L., Guldman, S. G., Matthews, J. C., Lander, R. H., Duffin, M. E., & Kyser, T. K. (1991). Clay mineral diagenesis in core KM-3 of Searles Lake, California. *Clays and Clay Minerals*, *39*(1), 84–96. https://doi.org/10.1346/CCMN.1991.0390111

Haywood, A. M., Dolan, A. M., Pickering, S. J., Dowsett, H. J., Mcclymont, E. L., Prescott, C. L., et al. (2013). On the identification of a Pliocene time slice for data-model comparison. *Philosophical Transactions of the Royal Society A: Mathematical, Physical and Engineering Sciences*, *371*(2001). https://doi.org/10.1098/rsta.2012.0515

Haywood, A. M., Dowsett, H. J., & Dolan, A. M. (2016). Integrating geological archives and climate models for the mid-Pliocene warm period. *Nature Communications 2016 7:1*, *7*(1), 1–14. https://doi.org/10.1038/ncomms10646

Haywood, A. M., Tindall, J. C., Dowsett, H. J., Dolan, A. M., Foley, K. M., Hunter, S. J., et al. (2020). The Pliocene Model Intercomparison Project Phase 2: large-scale climate features and climate sensitivity. *Climate of the Past*, *16*(6), 2095–2123.

Heusser, L. E. (1981). Pollen Analysis of Selected Samples from Deep Sea Drilling Project Leg 63 vol. 28. Initial Report of DSDP; 1981. p. 559–63. https://doi.org/10.2973/dsdp.proc.63.115.1981

Hildreth, W., Fierstein, J., & Calvert, A. T. (2018). McGee Till—oldest glacial deposit in the Sierra Nevada, California— and Quaternary evolution of the rangefront escarpment. *Quaternary Science Reviews*, *198*, 242–265. https://doi.org/10.1016/J.QUASCIREV.2018.08.008

Hopmans, E. C., Schouten, S., & Sinninghe Damsté, J. S. (2016). The effect of improved chromatography on GDGT-based palaeoproxies. *Organic Geochemistry*, *93*, 1–6. https://doi.org/10.1016/j.orggeochem.2015.12.006

Hren, M. T., Pagani, M., Erwin, D. M., & Brandon, M. (2010). Biomarker reconstruction of the early Eocene paleotopography and paleoclimate of the northern Sierra Nevada. *Geology*, *38*(1), 7–10. https://doi.org/10.1130/G30215.1

Huguet, C., Hopmans, E. C., Febo-Ayala, W., Thompson, D. H., Sinninghe Damsté, J. S., & Schouten, S. (2006). An improved method to determine the absolute abundance of glycerol dibiphytanyl glycerol tetraether lipids. *Organic Geochemistry*, *37*(9), 1036–1041. https://doi.org/10.1016/J.ORGGEOCHEM.2006.05.008

Ibarra, D. E., Oster, J. L., Winnick, M. J., Caves Rugenstein, J. K., Byrne, M. P., & Chamberlain, C. P. (2018). Warm and cold wet states in the western United States during the Pliocene–Pleistocene. *Geology*, *46*(4), 355–358. https://doi.org/10.1130/G39962.1

Jacobel, A. W., McManus, J. F., Anderson, R. F., & Winckler, G. (2016). Large deglacial shifts of the Pacific intertropical convergence zone. *Nature Communications*, *7*(1), 1–7.

Jayko, A. S., Forester, R. M., Kaufman, D. S., Phillips, F. M., Yount, J. C., McGeehin, J., & Mahan, S. A. (2008). Late Pleistocene lakes and wetlands, Panamint Valley, Inyo County, California. In *Special Paper of the Geological Society of America* (Vol. 439, pp. 151–184). https://doi.org/10.1130/2008.2439(07)

Jayko, A. S., Bacon, S. N., Reheis, M. C., Hershler, R., & Miller, D. M. (2008). Late Quaternary, MIS 6-8 shoreline features of pluvial Owens Lake, Owens Valley, eastern California. *SPECIAL PAPERS-GEOLOGICAL SOCIETY OF AMERICA*, *439*, 185.

Keisling, B. A., Castañeda, I. S., & Brigham-Grette, J. (2017). Hydrological and temperature change in Arctic Siberia during the intensification of Northern Hemisphere Glaciation. *Earth and Planetary Science Letters*, *457*, 136–148. https://doi.org/10.1016/J.EPSL.2016.09.058

Knott, J. R., Machette, M. N., Klinger, R. E., Sarna-Wojcicki, A. M., Liddicoat, J. C., Tinsley, J. C., et al. (2008). Reconstructing late Pliocene to middle Pleistocene Death Valley lakes and river systems as a test of pupfish (Cyprinodontidae) dispersal hypotheses. In *Special Paper of the Geological Society of America* (Vol. 439, pp. 1–26). Geological Society of America. https://doi.org/10.1130/2008.2439(01)

Knott, J. R., Machette, M. N., Wan, E., Klinger, R. E., Liddicoat, J. C., Sarna-Wojcicki, A. M., et al. (2018). Late Neogene–Quaternary tephrochronology, stratigraphy, and paleoclimate of Death Valley, California, USA. *GSA Bulletin*, *130*(7–8), 1231–1255. https://doi.org/10.1130/B31690.1

Knott, J. R., Wan, E., Deino, A. L., Casteel, M., Reheis, M. C., Phillips, F. M., et al. (2019). Lake Andrei: A pliocene pluvial lake in Eureka Valley, eastern California.

From Saline to Freshwater: The Diversity of Western Lakes in Space and Time, S. Starratt and MR Rosen, Eds, *536*, 125–142.

Knott, J. R., Liddicoat, J. C., Coe, R. S., & Negrini, R. M. (2021). Radiocarbon and paleomagnetic chronology of the Searles Lake Formation, San Bernardino County, California, USA. *From Saline to Freshwater: The Diversity of Western Lakes in Space and Time*, 81–95. https://doi.org/10.1130/2018.2536(06)

De La Vega, E., Chalk, T. B., Wilson, P. A., Bysani, R. P., & Foster, G. L. (2020). Atmospheric CO2 during the Mid-Piacenzian Warm Period and the M2 glaciation. *Scientific Reports*, *10*(1), 1–8.

Lachniet, M. S., Denniston, R. F., Asmerom, Y., & Polyak, V. J. (2014). Orbital control of western North America atmospheric circulation and climate over two glacial cycles. *Nature Communications*, *5*(1), 3805. https://doi.org/10.1038/ncomms4805

Liddicoat, J. C., Opdyke, N. D., & Smith, G. I. (1980). Palaeomagnetic polarity in a 930-m core from Searles Valley, California. *Nature*, *286*(5768), 22–25. https://doi.org/10.1038/286022a0

Lindberg, K. R., Daniels, W. C., Castañeda, I. S., & Brigham-Grette, J. (2022). Biomarker proxy records of Arctic climate change during the Mid-Pleistocene transition from Lake El'gygytgyn (Far East Russia). *Climate of the Past*, *18*(3), 559–577.

Lisiecki, L. E., & Raymo, M. E. (2005). A Pliocene-Pleistocene stack of 57 globally distributed benthic δ 18O records. *Paleoceanography*, *20*(1), 1–17. https://doi.org/10.1029/2004PA001071

Lofverstrom, M. (2020). A dynamic link between high-intensity precipitation events in southwestern North America and Europe at the Last Glacial Maximum. *Earth and Planetary Science Letters*, *534*, 116081.

Lora, J. M., Mitchell, J. L., Risi, C., & Tripati, A. E. (2017). North Pacific atmospheric rivers and their influence on western North America at the Last Glacial Maximum. *Geophysical Research Letters*, *44*(2), 1051-105.

Lowenstein, T. K., Dolginko, L. A. C., & García-Veigas, J. (2016). Influence of magmatic-hydrothermal activity on brine evolution in closed basins: Searles Lake, California. *Bulletin*, *128*(9–10), 1555–1568.

Mack, G. H., Giordano, T. H., Cole, D. R., James, W. C., & Salyards, S. L. (1994). Stable oxygen and carbon isotopes of pedogenic carbonate as indicators of Plio-Pleistocene paleoclimate in the southern Rio Grande Rift, south-central New Mexico. *American Journal of Science;(United States)*, *294*(5).

Martínez-Botí, M. A., Foster, G. L., Chalk, T. B., Rohling, E. J., Sexton, P. F., Lunt, D. J., et al. (2015). Plio-Pleistocene climate sensitivity evaluated using high-resolution CO2 records. *Nature*, *518*(7537), 49–54. https://doi.org/10.1038/nature14145

Martínez-Sosa, P., Tierney, J. E., Stefanescu, I. C., Dearing Crampton-Flood, E., Shuman, B. N., & Routson, C. (2021). A global Bayesian temperature calibration for lacustrine brGDGTs. *Geochimica et Cosmochimica Acta*, *305*, 87–105. https://doi.org/10.1016/J.GCA.2021.04.038

McClymont, E. L., Ho, S. L., Ford, H. L., Bailey, I., Berke, M. A., Bolton, C. T., ... & Tangunan, D. (2023). Climate Evolution through the onset and intensification of Northern Hemisphere Glaciation. *Reviews of Geophysics*, e2022RG000793.

McGee, D., Moreno-Chamarro, E., Marshall, J., & Galbraith, E. D. (2018a). Western U.S. lake expansions during Heinrich stadials linked to Pacific Hadley circulation. *Science Advances*, *4*(11). https://doi.org/10.1126/SCIADV.AAV0118/SUPPL_FILE/AAV0118_SM.PDF

McGee, D., Moreno-Chamarro, E., Marshall, J., & Galbraith, E. D. (2018b). Western U.S. lake expansions during Heinrich stadials linked to Pacific Hadley circulation. *Science Advances*, *4*(11), eaav0118. https://doi.org/10.1126/sciadv.aav0118

McPhillips, D., & Brandon, M. T. (2010). Using tracer thermochronology to measure modern relief change in the Sierra Nevada, California. *Earth and Planetary Science Letters*, *296*(3–4), 373–383. https://doi.org/10.1016/j.epsl.2010.05.022

Menemenlis, S., White, S. M., Ibarra, D. E., & Lora, J. M. (2022). A proxy-model comparison for mid-Pliocene warm period hydroclimate in the Southwestern US. *Earth and Planetary Science Letters*, *596*, 117803.

Mix, H. T., Ibarra, D. E., Mulch, A., Graham, S. A., & Page Chamberlain, C. (2016). A hot and high Eocene Sierra Nevada. *Bulletin of the Geological Society of America*, *128*(3–4), 531–542. https://doi.org/10.1130/B31294.1

Mix, H. T., Caves Rugenstein, J. K., Reilly, S. P., Ritch, A. J., Winnick, M. J., Kukla, T., & Chamberlain, C. P. (2019). Atmospheric flow deflection in the late Cenozoic Sierra Nevada. *Earth and Planetary Science Letters*, *518*, 76–85. https://doi.org/10.1016/j.epsl.2019.04.050

Molnar, P., & England, P. (1990). Late Cenozoic uplift of mountain ranges and global climate change: chicken or egg? *Nature 1990 346:6279*, *346*(6279), 29–34. https://doi.org/10.1038/346029a0

Moseley, G. E., Edwards, R. L., Wendt, K. A., Cheng, H., Dublyansky, Y., Lu, Y., et al. (2016). Reconciliation of the Devils Hole climate record with orbital forcing. *Science (New York, N.Y.)*, *351*(6269), 165–8. https://doi.org/10.1126/science.aad4132

Mulch, A., Sarna-Wojcicki, A. M., Perkins, M. E., & Chamberlain, C. P. (2008). A Miocene to Pleistocene climate and elevation record of the Sierra Nevada (California). *Proceedings of the National Academy of Sciences of the United States of America*, *105*(19), 6819–6824. https://doi.org/10.1073/pnas.0708811105

Ogg, J. G. (2020). Geomagnetic Polarity Time Scale. *Geologic Time Scale 2020*, 159–192. https://doi.org/10.1016/B978-0-12-824360-2.00005-X

Olson, K. J., & Lowenstein, T. K. (2021). Searles Lake evaporite sequences: Indicators of late Pleistocene/Holocene lake temperatures, brine evolution, and pCO2. *GSA Bulletin*. https://doi.org/10.1130/B35857.1

Olson, K. J., Guillerm, E., Peaple, M. D., Lowenstein, T. K., Gardien, V., Caupin, F., et al. (2023). Application of Brillouin thermometry to latest Pleistocene and Holocene halite from Searles Lake, California, USA. *Earth and Planetary Science Letters*, *602*, 117913.

Oster, J. L., Ibarra, D. E., Winnick, M. J., & Maher, K. (2015). Steering of westerly storms over western North America at the Last Glacial Maximum. *Nature Geoscience*, *8*(3), 201-205

Peaple, Mark D., Tierney, J. E., McGee, D., Lowenstein, T. K., Bhattacharya, T., & Feakins, S. J. (2021). Identifying plant wax inputs in lake sediments using machine learning. *Organic Geochemistry*, *156*, 104222. https://doi.org/10.1016/j.orggeochem.2021.104222

Peaple, Mark D., Bhattacharya, T., Lowenstein, T. K., McGee, D., Olson, K. J., Stroup, J. S., et al. (2022). Biomarker and Pollen Evidence for Late Pleistocene Pluvials in the Mojave Desert. *Paleoceanography and Paleoclimatology*, *37*(10), e2022PA004471. https://doi.org/10.1029/2022pa004471

Peaple, M.D.; Bhattacharya, T.; Tierney, J.E.; Knott, J.R.; Lowenstein, T.K.; Feakins, S.J. (2022-08-15): NOAA/WDS Paleoclimatology - Searles Valley Plant Wax Carbon and Hydrogen Isotopes and GDGTs during the Pliocene. [Dataset]. NOAA National Centers for Environmental Information. https://doi.org/10.25921/cmfc-b433

Post, F. J. (1977). The microbial ecology of the Great Salt Lake. *Microbial Ecology 1977 3:2*, *3*(2), 143–165. https://doi.org/10.1007/BF02010403

Qian, S., Yang, H., Dong, C., Wang, Y., Wu, J., Pei, H., et al. (2019). Rapid response of fossil tetraether lipids in lake sediments to seasonal environmental variables in a shallow lake in central China: Implications for the use of tetraether-based proxies. *Organic Geochemistry*, *128*, 108–121.

Ravelo, A. C., Andreasen, D. H., Lyle, M., Olivarez Lyle, A., & Wara, M. W. (2004). Regional climate shifts caused by gradual global cooling in the Pliocene epoch. *Nature*, *429*(6989), 263–267.

Raymo, M. E., Kozdon, R., Evans, D., Lisiecki, L., & Ford, H. L. (2018). The accuracy of mid-Pliocene δ18O-based ice volume and sea level reconstructions. *Earth-Science Reviews*, *177*, 291–302. https://doi.org/10.1016/J.EARSCIREV.2017.11.022

Reheis, M. C., Slate, J. L., Sarna-Wojcicki, A. M., & Meyer, C. E. (1993). A late Pliocene to middle Pleistocene pluvial lake in Fish Lake Valley, Nevada and California. *Geological Society of America Bulletin*, *105*(7), 953–967.

Remeika, P., Fischbein, I. W., & Fischbein, S. A. (1988). Lower Pliocene petrified wood from the Palm Spring Formation, Anza Borrego Desert State Park, California. *Review of Palaeobotany and Palynology*, *56*(3–4), 183–198. https://doi.org/10.1016/0034-6667(88)90057-7

Rittase, W. M., Walker, J. D., Andrew, J., Kirby, E., & Wan, E. (2020). Pliocene–Pleistocene basin evolution along the Garlock fault zone, Pilot Knob Valley, California. *Geosphere*, *16*(5), 1208–1224. https://doi.org/10.1130/GES02209.1Russell, I. C. (1885). Geological history of Lake Lahontan, a Quaternary lake of northwestern Nevada. *Monographs of the United States Geological Survey*. https://doi.org/10.3133/m11

Sánchez-Montes, M. L., McClymont, E. L., Lloyd, J. M., Müller, J., Cowan, E. A., & Zorzi, C. (2020). Late Pliocene Cordilleran Ice Sheet development with warm northeast Pacific sea surface temperatures. *Climate of the Past*, *16*(1), 299-313

De Schepper, S., Gibbard, P. L., Salzmann, U., & Ehlers, J. (2014). A global synthesis of the marine and terrestrial evidence for glaciation during the Pliocene Epoch. *Earth-Science Reviews*, *135*, 83–102.

Schouten, S., Hopmans, E. C., Schefuß, E., & Sinninghe Damsté, J. S. (2002). Distributional variations in marine crenarchaeotal membrane lipids: a new tool for reconstructing ancient sea water temperatures? *Earth and Planetary Science Letters*, *204*, 265–274. https://doi.org/10.1016/S0012-821X(03)00193-6

Seager, R., Ting, M., Held, I., Kushnir, Y., Lu, J., Vecchi, G., et al. (2007). Model projections of an imminent transition to a more arid climate in southwestern North America. *Science*, *316*(5828), 1181–1184.

Shackleton, N. J., & Opdyke, N. D. (1977). Oxygen isotope and palaeomagnetic evidence for early Northern Hemisphere glaciation. *Nature*, *270*(5634), 216–219.

Smith, G. I. (2009). Late Cenozoic geology and lacustrine history of Searles Valley, Inyo and San Bernardino counties, California. *US Geological Survey Professional Paper*. https://doi.org/10.3133/pp1727

Smith, G.I. (1991). Stratigraphy and chronology of Quaternary-age lacustrine deposits. *Quaternary nonglacial geology: Conterminous U.S.*, Morrison, R.B., ed., 339-352.

Smith, G. I., Barczak, V. J., Moulton, G. F., & Liddicoat, J. C. (1983). *Core KM-3, a surface-to-bedrock record of late Cenozoic sedimentation in Searles Valley, California*. *Professional Paper*. https://doi.org/10.3133/PP1256

So, R. T., Lowenstein, T. K., Jagniecki, E., Tierney, J. E., & Feakins, S. J. (2023). Holocene water balance variations in Great Salt Lake, Utah: Application of GDGT indices and the ACE salinity proxy. *Paleoceanography and Paleoclimatology, 38, e2022PA004558.* https://doi.org/10.1029/2022PA004558

Solomon, S., Plattner, G.-K., Knutti, R., & Friedlingstein, P. (2009). Irreversible climate change due to carbon dioxide emissions. *Proceedings of the National Academy of Sciences*, *106*(6), 1704–1709.

Stock, G. M., Anderson, R. S., & Finkel, R. C. (2004). Pace of landscape evolution in the Sierra Nevada, California, revealed by cosmogenic dating of cave sediments. *Geology*, *32*(3), 193–196. https://doi.org/10.1130/G20197.1

Stroup, J. S., Olson, K. J., Lowenstein, T. K., Jost, A. B., Mosher, H. M., Peaple, M. D., et al. (2023). A >200 ka U-Th Based Chronology from Lacustrine Evaporites, Searles Lake, CA. *Geochemistry, Geophysics, Geosystems*, *24*(3), e2022GC010685. https://doi.org/https://doi.org/10.1029/2022GC010685

Tan, N., Ramstein, G., Dumas, C., Contoux, C., Ladant, J.-B., Sepulchre, P., et al. (2017). Exploring the MIS M2 glaciation occurring during a warm and high atmospheric CO2 Pliocene background climate. *Earth and Planetary Science Letters*, *472*, 266–276.

Thompson, R. S. (1991). Pliocene environments and climates in the western United States. *Quaternary Science Reviews*, *10*(2–3), 115–132. https://doi.org/10.1016/0277-3791(91)90013-K

Tierney, J. E., & Tingley, M. P. (2018). BAYSPLINE: A New Calibration for the Alkenone Paleothermometer. *Paleoceanography and Paleoclimatology*, *33*(3), 281–301. https://doi.org/10.1002/2017PA003201

Western Regional Climate Center. (2022). *Cooperative Climatological Data Summaries* Retrieved from https://wrcc.dri.edu/cgi-bin/cliMAIN.pl?ca9035

Truong, C., Oudre, L., & Vayatis, N. (2020). Selective review of offline change point detection methods. *Signal Processing*, *167*, 107299. https://doi.org/10.1016/j.sigpro.2019.107299

Turich, C., & Freeman, K. H. (2011). Archaeal lipids record paleosalinity in hypersaline systems. *Organic Geochemistry*, *42*(9), 1147–1157. https://doi.org/10.1016/J.ORGGEOCHEM.2011.06.002

Wambui, G. D., Waititu, G. A., & Wanjoya, A. (2015). The power of the pruned exact linear time (PELT) test in multiple changepoint detection. *American Journal of*

Theoretical and Applied Statistics, *4*(6), 581. https://doi.org/10.11648/j.ajtas.20150406.30Walker, J. D., Bidgoli, T. S., Didericksen, B. D., Stockli, D. F., & Andrew, J. E. (2014). Middle Miocene to recent exhumation of the Slate Range, eastern California, and implications for the timing of extension and the transition to transtension. *Geosphere*, *10*(2), 276–291. https://doi.org/10.1130/GES00947.1

Wang, H., Liu, W., He, Y., Zhou, A., Zhao, H., Liu, H., et al. (2021). Salinity-controlled isomerization of lacustrine brGDGTs impacts the associated MBT_{5ME}' terrestrial temperature index. *Geochimica et Cosmochimica Acta*, *305*, 33–48. https://doi.org/10.1016/J.GCA.2021.05.004

Wang, Y., Cerling, T. E., Quade, J., Bowman, J. R., Smith, G. A., & Lindsay, E. H. (1993). Stable isotopes of paleosols and fossil teeth as paleoecology and paleoclimate indicators: an example from the St. David Formation, Arizona. *Washington DC American Geophysical Union Geophysical Monograph Series*, *78*, 241–248.

Westerhold, T., Marwan, N., Drury, A. J., Liebrand, D., Agnini, C., Anagnostou, E., et al. (2020). An astronomically dated record of Earth's climate and its predictability over the last 66 million years. *Science*, *369*(6509), 1383–1387.

Western Regional Climate Center. (2013). *Cooperative Climatological Data Summaries*. Retrieved from https://wrcc.dri.edu/

William C. Daniels, Isla S. Castañeda, Jeffrey M. Salacup, M. Helen Habicht, Kurt R. Lindberg, Julie Brigham-Grette. 2022 Archaeal lipids reveal climate-driven changes in microbial ecology at Lake El'gygytgyn (Far East Russia) during the Plio-Pleistocene. "Journal of Quaternary Science ", vol 37, number 5, 900-914

Williams, A. P., Cook, E. R., Smerdon, J. E., Cook, B. I., Abatzoglou, J. T., Bolles, K., et al. (2020). Large contribution from anthropogenic warming to an emerging North American megadrought. *Science*, *368*(6488), 314–318. https://doi.org/10.1126/SCIENCE.AAZ9600

Winters, Y. D., Lowenstein, T. K., & Timofeeff, M. N. (2013). Identification of Carotenoids in Ancient Salt from Death Valley, Saline Valley, and Searles Lake, California, Using Laser Raman Spectroscopy. *Astrobiology*, *13*(11), 1065–1080. https://doi.org/10.1089/ast.2012.0952

Wu, J., Yang, H., Pancost, R. D., Naafs, B. D. A., Qian, S., Dang, X., et al. (2021). Variations in dissolved O2 in a Chinese lake drive changes in microbial communities and impact sedimentary GDGT distributions. *Chemical Geology*, *579*, 120348.

Wu, M. S., West, A. J., & Feakins, S. J. (2019). Tropical soil profiles reveal the fate of plant wax biomarkers during soil storage. *Organic Geochemistry*, *128*, 1–15. https://doi.org/10.1016/j.orggeochem.2018.12.011

References from the supporting information

Mix, H. T., Caves Rugenstein, J. K., Reilly, S. P., Ritch, A. J., Winnick, M. J., Kukla, T., & Chamberlain, C. P. (2019). Atmospheric flow deflection in the late Cenozoic Sierra Nevada. *Earth and Planetary Science Letters*, *518*, 76–85. https://doi.org/10.1016/j.epsl.2019.04.050

Jennings, C.W., 1977, Geologic Map of California: California Geological Survey Geologic Data Map No. 2; https://maps.conservation.ca.gov/cgs/gmc/.

Cox, B.F., Hillhouse, J.W., and Owen, L.A., 2003, Pliocene and Pleistocene evolution of the Mojave River, and associated tectonic development of the Transverse Ranges and Mojave Desert, based on borehole stratigraphy studies and mapping of landforms and sediments near Victorville, California, in Enzel, Y., Wells, S.G., and Lancaster, N., eds., Paleoenvironments and paleohydrology of the Mojave and southern Great Basin Deserts: Boulder, Colorado, Geological Society of America Special Paper 368, p. 1-42.

Knott, J.R., Machette, M.N., Wan, E., Klinger, R.E., Liddicoat, J.C., Sarna-Wojcicki, A.M., Fleck, R.J., Deino, A.L., Geissman, J.W., Slate, J.L., Wahl, D.B., Wernicke, B.P., Wells, S.G., Tinsley, J.C. III, Hathaway, J.C., and Weamer, V.M., 2018. Late Neogene-Quaternary tephrochronology, stratigraphy and paleoclimate of Death Valley, CA, U.S.A. Geological Society of America Bulletin 130 (7/8), 1231-1255, doi.org/10.1130/B31690.1.

Knott, J.R., Sarna-Wojcicki, A.M., Meyer, C.E., Tinsley, J.C., III, Wells, S.G., and Wan, E., 1999. Late Cenozoic stratigraphy and tephrochronology of the western Black Mountains piedmont, Death Valley, California: Implications for the tectonic development of Death Valley. In Wright, L.A., and Troxel, B.W., (Eds.), Cenozoic Basins of the Death Valley Region, Volume Special Paper 333: Geological Society of America, 345-366, doi:10.1130/0-8137-2333-7.345.

Knott, J.R., Liddicoat, J.C., Coe, R.S., and Negrini, R.M., 2019a. Radiocarbon and paleomagnetic chronology of the Searles Lake Formation, San Bernardino County, California, U.S.A. In, Starratt, S.W. and Rosen, M.R., (Eds.), From Saline to Freshwater: The Diversity of Western Lakes in Space and Time: Geological Society of America Special Paper 536, 81-95, doi.org/10.1130/2018.2536(06).

Knott, J.R., Wan, E., Deino, A.L., Casteel, M., Reheis, M.C., Phillips, F.M., Walkup, L., McCarty, K., Manoukian, D.N., and Nunez, E., 2019b. Lake Andrei: A Pliocene pluvial lake in Eureka Valley, eastern California. In Starratt, S.W. and Rosen, M.R., (Eds.), From Saline to Freshwater: The Diversity of Western Lakes in Space and Time: Geological Society of America Special Paper 536, 125-142, doi.org/10.1130/2018.2536(08).

Lutz, B., Knott, J.R., Phillips, F., Heizler, M.T., Heitkamp, K.A., Jr., Griffie, E.L., Asxen, G.A. and Calzia, J.P., 2022. Tectonically controlled drainage fragmentation in the southwestern Great Basin, USA. Geological Society of America Bulletin, doi: 10.1130/B36563.1.

Table and Figure captions:

Table 1. Summary of the key findings

Name	Age (Ma)	T (ºC)	Salinity	P-E	δD$_{precip}$ (‰)	δ^{13}C (‰)
MIS M2-pluvial	3.370-3.264	21±3	Low	Much wetter than modern	Unchanged	Unchanged
Extended mPWP	3.264-2.950	25±3	Moderate	Slightly wetter than modern	Unchanged	Unchanged

Figure 1. a) Map of southwestern North America showing Searles Lake (star) and other late Pliocene sites (circles) referred to in this study. Light grey lines represent USA state boundaries. b) Map of the western Great Basin region highlighting late Pliocene sites and the location of the Sierra Nevada (mountain range). Catchment of Pliocene Searles Valley highlighted in yellow and calculated using the 90 m Copernicus digital elevation model (European Space Agency, Sinergise 2021). c) Map of local Searles Valley region, highlighting tectonic features related to the development of Searles Valley. KM3 core site represented by an orange star.

Figure 2. a) Age model generated using BACON (black line), 95% confidence interval (grey shading) and paleomagnetic datums (Liddicoat et al., 1980) updated to the GPTS2020 (Channell et al., 2020; Ogg, 2020) (red circles). This study focused on the late Pliocene perennial lake phase (blue shading), terminating 18 m below the Gauss-Matuyama boundary (labelled G/M, 522.9 m, 2.606 Ma, 3 ka 1σ) (Liddicoat et al., 1980; Smith et al., 1983). Left: Reconstructed Searles Lake environment (Smith et al., 1983). Right: Paleomagnetic reversals. b) Section of age model covering samples in this study. Tuffs at 681.5 m and 693.4 m (blue crosses) correlate with tuffs of Mesquite Spring (3.3032 +/- 0.0025 Ma; Deino et al., 2018) and Zabriskie Wash (3.335 +/- 0.002 Ma; Knott et al., 2018) in Death Valley providing independent age constraints.

Figure 3. Searles Lake proxy reconstructions for the Late Pliocene. Comparison of a) summary of lake depth from Eureka Valley's Lake Andrei (Knott et al., 2019), Death Valley (Knott et al., 2018), and Searles Lake (Smith et al., 1983). b) Global composite record of benthic foraminiferal carbonate $\delta^{18}O$ binned, resampled and smoothed with a locally weighted function to 20 ka resolution (Westerhold et al., 2020). Searles Lake proxy reconstructions from core KM-3 (this study) including: c) ∑brGDGT and ∑isoGDGT concentrations (note different axes), d) ACE and IR_{6+7Me} indices of salinity, e) $BayMBT_0$ temperature reconstruction of mean air temperature for months above freezing, f) $\sum C_{22-32}$ alkanoic acid concentration and Average chain length (ACL) of *n*-alkanoic acids, g) $\delta^{13}C$ value of C_{28} *n*-alkanoic acid (light green) and C_{30} *n*-alkanoic acid (dark green), and h) δD value of precipitation (light and dark blue as for h). Blue shading represents Searles Lake deep lake period (3.370–3.264 Ma) overlapping with the Mammoth reverse chron. Yellow shading represents the extended mid-Pliocene warm period (3.264–2.950 Ma). Paleomagnetic age boundaries are shown on the x axis. GDGT indices only reported when numerator and denominator peaks present.

Figure 4. Global and regional context for comparison to Searles Lake GDGT proxy reconstructions for the Late Pliocene. a) Summary of Eureka Valley, Death Valley and Searles Valley paleoenvironments. b) Global composite record of benthic foraminiferal carbonate $\delta^{18}O$ binned, resampled and smoothed with a locally weighted function to 20 ka resolution (Westerhold et al., 2020). Annotated with the names of the MIS MG4, MG2 and M2 glacial events. c) Lake El'gygtgyn, Siberia, mean temperature of warmest month (MTWM) reconstructed from pollen compared to modern (Brigham-Grette et al., 2013). d) Sea surface temperatures (SSTs) from alkenone Uk'_{37} index in the Gulf of Alaska (Sánchez-Montes et al., 2020) and ODP 1012 (Brierley et al., 2009) recalibrated using BAYSPLINE (Tierney & Tingley, 2018). Select Searles Lake proxy reconstructions from core KM-3 (this study) including: e) $BayMBT_0$ temperature reconstruction of mean air temperature for months above freezing (MAF) compared to modern (solid line), f) ACE index of salinity g) IR_{6+7Me} index of salinity. Change points (red lines) calculated using the Pruned Extract Linear Time algorithm using the Ruptures Python package (Truong et al., 2020). Shading and age control as in Figure 3.

Figure 5. Violin plots showing distributions of reconstructed $BayMBT_0$ temperatures (months above freezing) from Searles Lake sediments. Left panel shows previously published (Peaple et al., 2022) temperatures from the last and penultimate glacial maxima (GM) as well as the last interglacial (LIG). Right panel (this study) show temperatures from the M2 glaciation (M2) and the mid Pliocene warm period (mPWP).

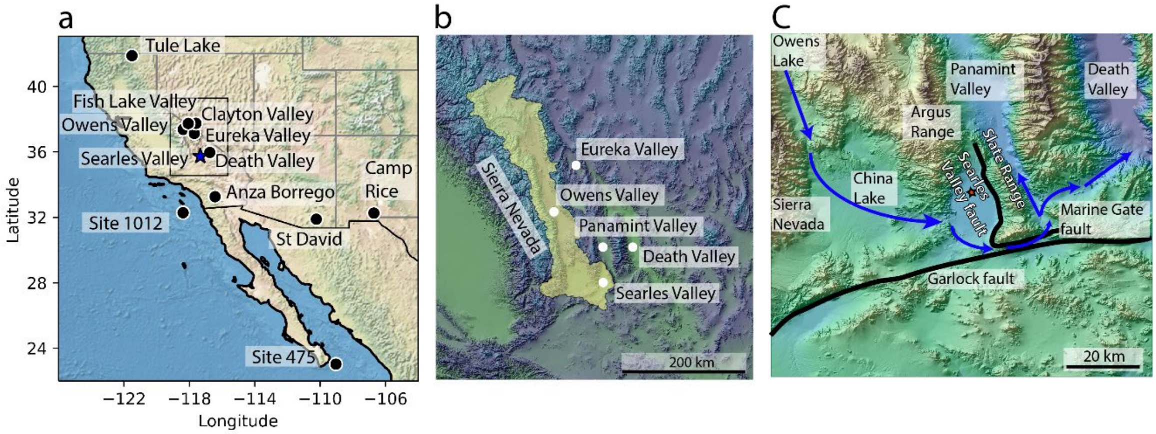
a
b
C
Tule Lake
Fish Lake Valley
Owens Valley
Clayton Valley
Eureka Valley
Searles Valley
Death Valley
Camp Rice
Anza Borrego
Site 1012
St David
Site 475
Latitude
Longitude
Sierra Nevada
Panamint Valley
200 km
Owens Lake
Argus Range
China Lake
Slate Range
Searles Valley fault
Marine Gate fault
Garlock fault
20 km

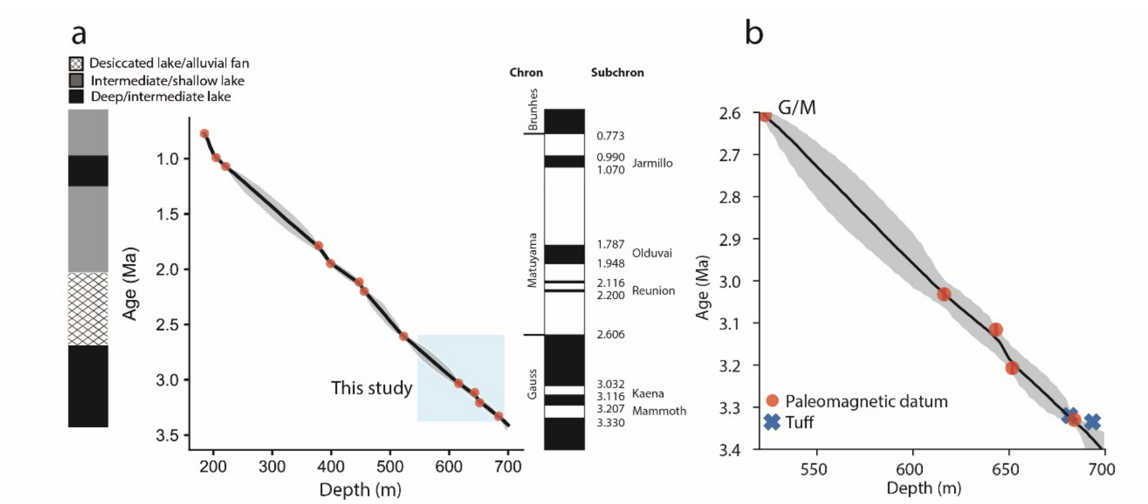
a
b
Desiccated lake/alluvial fan
Intermediate/shallow lake
Deep/intermediate lake
Age (Ma)
Depth (m)
This study
Chron
Subchron
Brunhes
Matuyama
Gauss
Jarmillo
Olduvai
Reunion
Kaena
Mammoth
G/M
Paleomagnetic datum
Tuff

1337

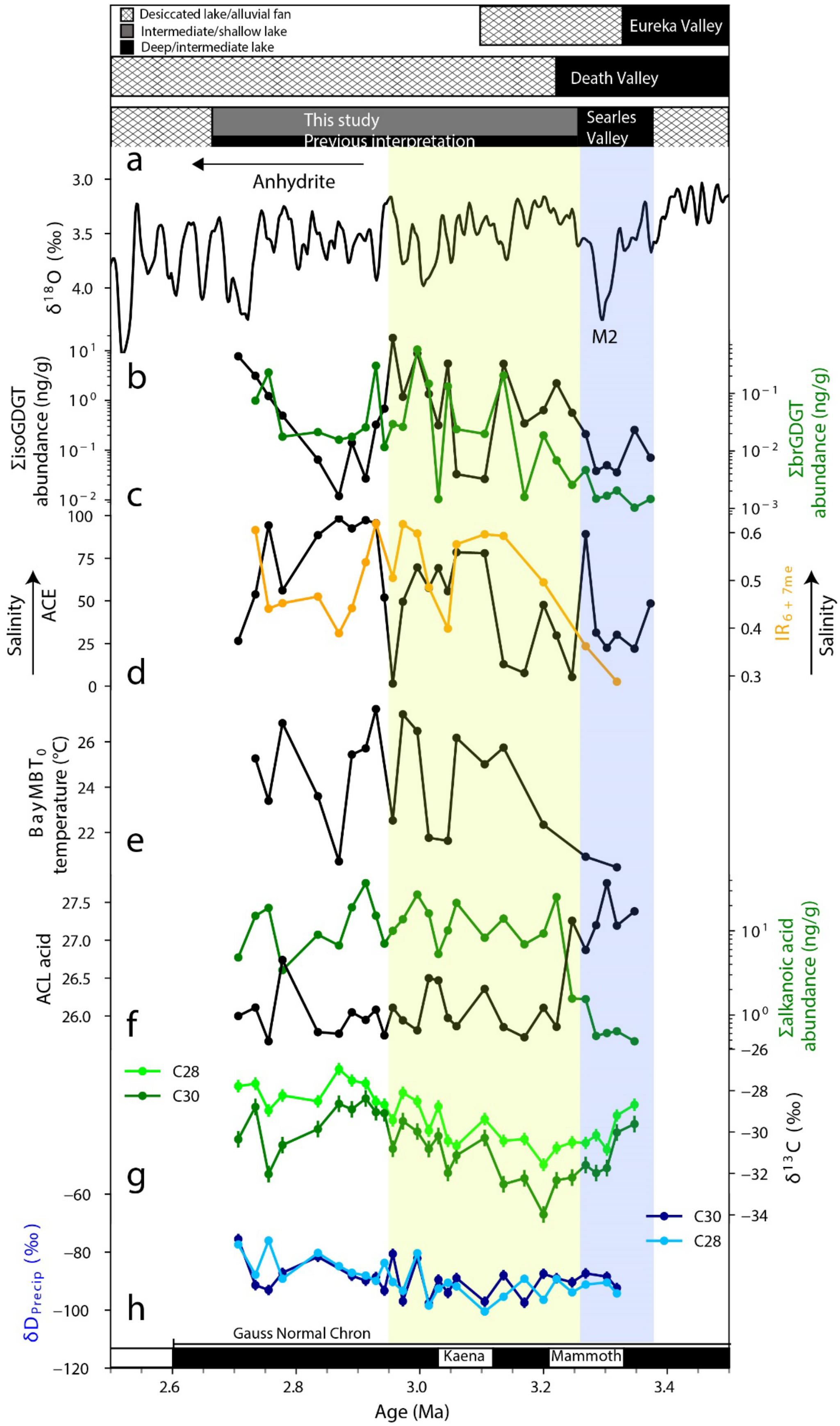
Desiccated lake/alluvial fan
Intermediate/shallow lake
Deep/intermediate lake
Eureka Valley
Death Valley
This study
Previous interpretation
Searles Valley
a
Anhydrite
δ18O (‰)
M2
ΣisoGDGT abundance (ng/g)
ΣbrGDGT abundance (ng/g)
b
c
Salinity
ACE
IR6+7me
d
BayMBT0 temperature (°C)
e
ACL acid
Σalkanoic acid abundance (ng/g)
f
C28
C30
δ13C (‰)
g
δDPrecip (‰)
h
Gauss Normal Chron
Kaena
Mammoth
Age (Ma)

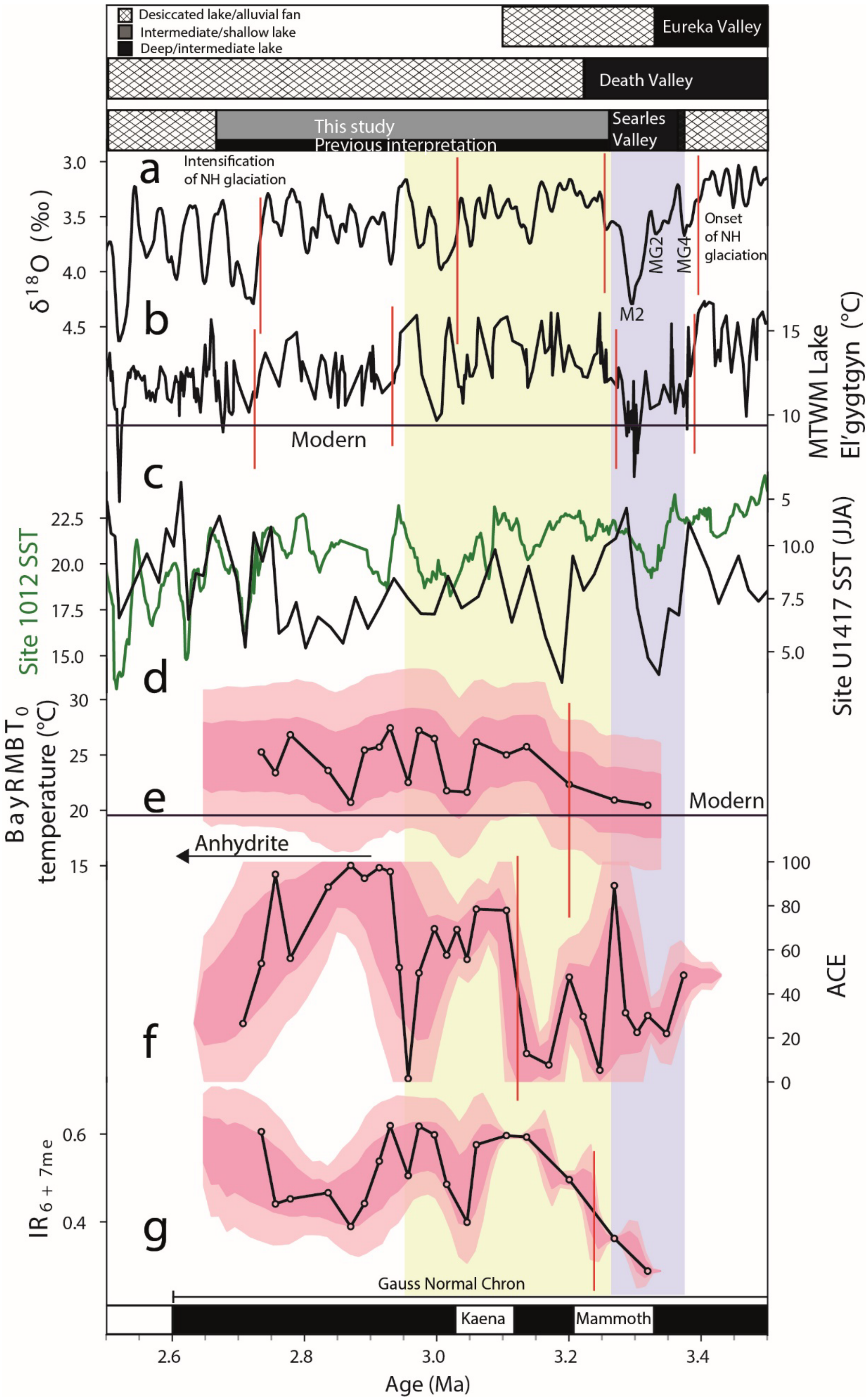

Desiccated lake/alluvial fan
Intermediate/shallow lake
Deep/intermediate lake
Eureka Valley
Death Valley
This study
Previous interpretation
Searles Valley
a
Intensification of NH glaciation
Onset of NH glaciation
MG2
MG4
M2
b
Modern
c
d
e
Modern
Anhydrite
f
g
Gauss Normal Chron
Kaena
Mammoth
δ18O (‰)
MTWM Lake El'gygytgyn (°C)
Site 1012 SST
Site U1417 SST (JJA)
BayRMBT0 temperature (°C)
ACE
IR6 + 7me
Age (Ma)

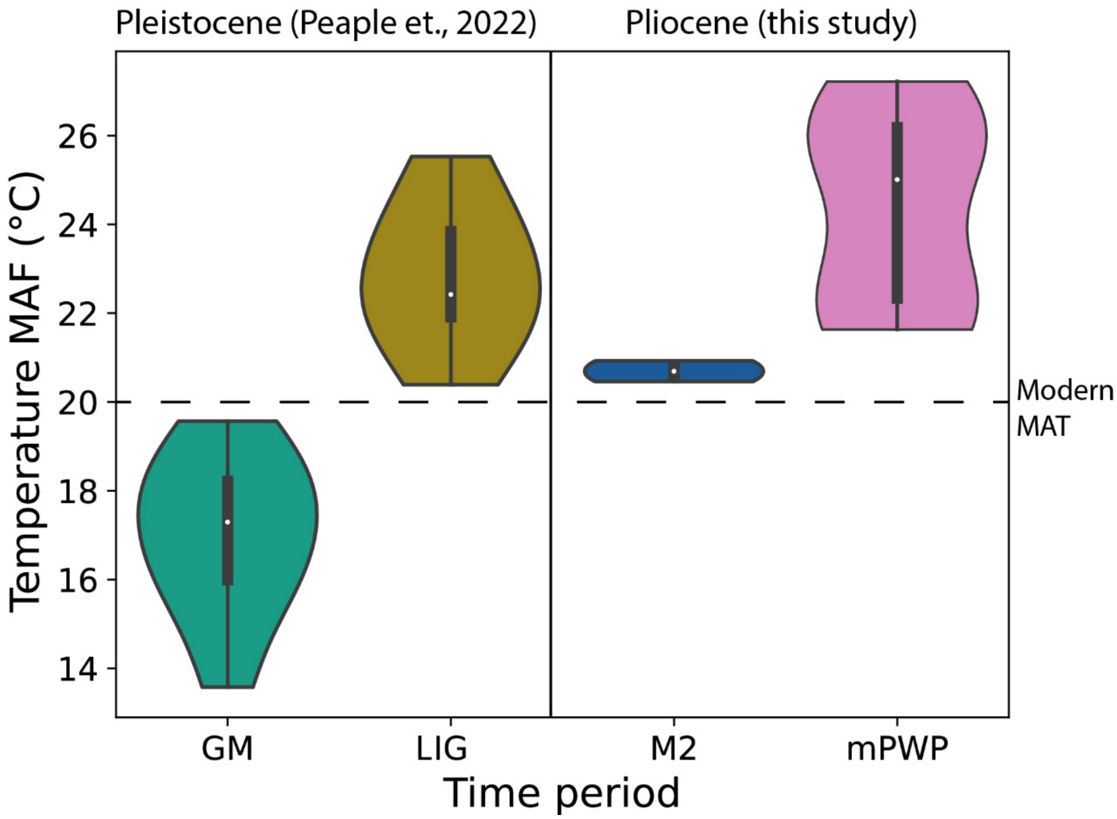
Pleistocene (Peaple et., 2022)
Pliocene (this study)
Temperature MAF (°C)
26
24
22
20
18
16
14
Modern
MAT
GM
LIG
M2
mPWP
Time period